

# Scalar Resonances near 650 and 95 GeV in the GNMSSM with Correct Dark Matter Relic Abundance

---

Jingwei Lian<sup>\*1,2</sup>, Yao-Bei Liu<sup>1</sup>

<sup>1</sup>*Henan Institute of Science and Technology, Xinxiang 453003, P.R. China*

<sup>2</sup>*School of Physics, Henan Normal University, Xinxiang 453007, P.R. China*

*E-mail:* [lianjw@hist.edu.cn](mailto:lianjw@hist.edu.cn), [liuyaobei@hist.edu.cn](mailto:liuyaobei@hist.edu.cn)

ABSTRACT: Recent CMS analyses report an excess in the diphoton-plus- $b\bar{b}$  channel, indicative of a heavy resonance around 650 GeV decaying into a Standard Model (SM)-like Higgs boson and a lighter scalar near 95 GeV. The case for a 95 GeV state is further supported by diphoton excesses observed by both CMS and ATLAS, as well as a  $b\bar{b}$  excess previously observed at the Large Electron-Positron collider. This study presents a unified interpretation of these anomalies within the framework of the General Next-to-Minimal Supersymmetric Standard Model that naturally accommodates a light singlet-dominated  $CP$ -even scalar boson  $h_s$  near 95 GeV and a heavier doublet-like scalar boson  $A_H$  near 650 GeV. Through a comprehensive scan of the parameter space, we demonstrate that the model can explain these excesses at  $2\sigma$  level while satisfying constraints from the dark matter relic density, direct detection experiments, the properties of the 125 GeV Higgs boson,  $B$ -physics observables, and searches for electroweakinos at the Large Hadron Collider (LHC). The interpretation features a Bino-dominated lightest neutralino as the dark matter candidate, whose relic abundance is achieved primarily via  $A_s$  funnel annihilation or coannihilation with  $\tilde{S}$ -like  $\tilde{\chi}_2^0$ s into  $h_s A_H$  final states. Our findings provide clear predictions for testing this scenario at the high-luminosity LHC and future colliders.

---

<sup>\*</sup>Corresponding author.

---

## Contents

<b>1</b>	<b>Introduction</b>	<b>1</b>
<b>2</b>	<b>Theoretical preliminaries</b>	<b>3</b>
2.1	The Superpotential of the GNMSSM	3
2.2	Higgs Sector	4
2.3	Neutralino Sector	6
<b>3</b>	<b>Explanation of the excesses</b>	<b>7</b>
3.1	Strategy in scanning the parameter space	7
3.2	Numerical Results	10
<b>4</b>	<b>Conclusion</b>	<b>20</b>
<b>A</b>	<b>Appendix</b>	<b>22</b>

---

## 1 Introduction

The monumental discovery of the Higgs boson at the Large Hadron Collider (LHC) in 2012 confirmed the existence of a scalar field responsible for electroweak symmetry breaking (EWSB) and mass generation. Although the measured properties of the 125 GeV Higgs boson are broadly consistent with Standard Model (SM) predictions, persistent theoretical issues—most notably the hierarchy problem—continue to motivate the exploration of physics beyond the Standard Model (BSM). Supersymmetry (SUSY) remains a compelling BSM framework, as it provides a natural solution to the hierarchy problem and typically necessitates an extended Higgs sector that predicts the existence of additional scalar states. The search for these new states is paramount, as their observation would provide essential insights into the structure of EWSB and the realization of BSM models.

Intriguingly, several collider experiments have reported persisting hints of such additional scalar states. The first suggestion emerged from LEP experiments, where combined searches for the SM Higgs boson revealed a mild excess in the process  $e^+e^- \rightarrow Z^* \rightarrow Z + b\bar{b}$  for Higgs masses in the range 95-100 GeV. This corresponded to a local significance of  $2.3\sigma$  and a signal strength [1–3]:

$$\mu_{b\bar{b}}^{\text{exp}} = 0.117 \pm 0.057. \quad (1.1)$$

This initial hint gained traction with a subsequent observation by CMS at the LHC, which reported an excess in the diphoton ( $\gamma\gamma$ ) channel near 97 GeV during Run 1, carrying a local significance of approximately  $2\sigma$  [4]. Most recently, the case for this light scalar has been significantly reinforced using the full Run 2 dataset. Both the CMS and ATLAS collaborations, employing advanced analysis techniques, have observed a consistent excess

at an invariant mass of  $m_{\gamma\gamma} = 95.4$  GeV [5, 6]. The combined signal strength is now interpreted as a  $3.1\sigma$  local excess with a signal rate [7]:

$$\mu_{\gamma\gamma}^{\text{exp}} \equiv \mu_{\gamma\gamma}^{\text{ATLAS+CMS}} = \frac{\sigma(pp \rightarrow \phi \rightarrow \gamma\gamma)}{\sigma_{\text{SM}}(gg \rightarrow H_{\text{SM}} \rightarrow \gamma\gamma)} = 0.24_{-0.08}^{+0.09}, \quad (1.2)$$

where,  $\phi$  denotes a hypothetically non-SM scalar with mass  $m_\phi = 95.4$  GeV responsible for the diphoton excess, and  $\sigma_{\text{SM}}$  refers to the cross section expected for an SM-like Higgs boson  $H_{\text{SM}}$  of the same mass. Additional phenomenological support for an about 95 GeV state arises from a mild surplus in the di- $\tau$  channel observed by CMS [8] and a potential excess in  $WW$  final states [9]. Collectively, these observations strengthen the case for the existence of a light scalar resonance around 95 GeV.

Complementing these hints at low mass, a recent search by CMS has unveiled an inter-connected anomaly — a  $3.8\sigma$  local excess in the search channel featuring a diphoton a diphoton and a  $b\bar{b}$  pair. This signal is attributed to the decay of a heavy resonance  $X$  near 650 GeV into a SM-like Higgs boson and a BSM scalar  $\phi$  in the 90–100 GeV mass range [10]. The observed production cross section times branching fraction is [11]:

$$\sigma_{\gamma\gamma b\bar{b}} = \sigma(gg \rightarrow X \rightarrow H_{\text{SM}}(\gamma\gamma) + \phi(b\bar{b})) = 0.35_{-0.13}^{+0.17} \text{ fb}. \quad (1.3)$$

It is critical to consider constraints from complementary final states. Specifically, a prior CMS search in the  $\tau\bar{\tau}$  plus  $b\bar{b}$  channel [12] imposes a stringent upper 95% CL limit of approximately 3 fb on the cross section  $\sigma(X \rightarrow H_{\text{SM}}(\tau\bar{\tau}) + \phi(b\bar{b}))$ . This translates into an upper 95% CL limit of about 0.1 fb on  $\sigma_{\gamma\gamma b\bar{b}}$  [11], suggesting a tension between the observed excess and current limits from related channels.

These collective anomalies have sparked extensive investigations across various BSM scenarios [3, 7, 11, 13–82]. In particular, several works [11, 44, 54, 75–77] have explored the possible connection between the 95 GeV and 650 GeV excesses. Among the proposed explanations, the Next-to-Minimal Supersymmetric Standard Model (NMSSM) [83–89] stands out as a particularly attractive and economical framework for accommodating these scalar states and furnishing proper dark matter (DM) candidates. Previous NMSSM studies with a  $\mathbb{Z}_3$  symmetry have investigated both mass excesses [11, 90], though typically under the assumption that the observed DM relic density receives additional contributions beyond the lightest supersymmetric particle (LSP). The general form of the NMSSM, termed as “GNMSSM”, includes  $\mathbb{Z}_3$ -violating terms that naturally address the tadpole and domain-wall problems [88]. The enlarged parameter space, featuring ten parameters in the Higgs sector, offers the necessary flexibility to account for both the 95 GeV and 650 GeV excesses, while also providing a rich phenomenology for the Singlino/Bino DM sector. The  $\mathbb{Z}_3$ -breaking terms also modify the Higgsino and Singlino masses, significantly influencing the DM sector. Our recent work [51, 60] has shown that the 95 GeV excesses can be consistently explained in the GNMSSM through a Singlino-dominated LSP that saturates the observed DM relic density without violating existing experimental constraints.

The goal of this paper is to determine to what extent the 95 GeV and 650 GeV excesses can be simultaneously explained within the GNMSSM while remaining compatible with current LHC data and the recent null results from the LZ dark-matter experiment. In

this framework, the heavy CP-even Higgs boson with mass near 650 GeV decays into a SM-like Higgs boson and a light singlet-dominated CP-even Higgs boson with mass around 95 GeV. We demonstrate that the GNMSSM can simultaneously account for the LEP, CMS, and ATLAS hints of a 95 GeV scalar as well as the CMS diphoton plus  $b\bar{b}$  excess near 650 GeV at the  $2\sigma$  level. We further identify parameter regions in which a Bino-dominated neutralino constitutes a viable thermal DM candidate, potentially testable by the forthcoming sensitivity of direct-detection experiments.

The remainder of this paper is organized as follows. In Sec. 2, we briefly recapitulate the basics of the GNMSSM framework and the predicted signal rates for the anomalies. In Sec. 3, we perform a sophisticated scan over the model parameter space and present detailed numerical results. Finally, our conclusions are summarized in Sec. 4.

## 2 Theoretical preliminaries

### 2.1 The Superpotential of the GNMSSM

The NMSSM is known as a straightforward and well-motivated extension of the Minimal Supersymmetric Standard Model (MSSM), achieved by introducing a gauge-singlet chiral superfield [83–87]. Its appeal stems not only from providing a natural solution to the so-called  $\mu$ -problem inherent in the MSSM, but also from offering an expanded and often more viable DM sector [91–93]. Crucially, the NMSSM contributes to a sizeable mass lift for the SM-like Higgs boson. Especially in scenarios involving a light CP-even Higgs, this mass can be elevated by both an additional tree-level contribution and a large singlet-doublet mixing [94–96], mitigating the need for substantial radiative corrections from top/stop loops. The GNMSSM incorporates the most general renormalizable couplings in its superpotential [88]

$$W_{\text{GNMSSM}} = W_{\text{Yukawa}} + \lambda \hat{S} \hat{H}_u \cdot \hat{H}_d + \frac{\kappa}{3} \hat{S}^3 + \mu \hat{H}_u \cdot \hat{H}_d + \frac{1}{2} \mu' \hat{S}^2 + \xi \hat{S}, \quad (2.1)$$

where  $W_{\text{Yukawa}}$  contains the quark and lepton Yukawa terms in the MSSM superpotential,  $\hat{H}_u = (\hat{H}_u^+, \hat{H}_u^0)^T$  and  $\hat{H}_d = (\hat{H}_d^0, \hat{H}_d^-)^T$  are the  $SU(2)_L$  Higgs doublet superfields, and  $\hat{S}$  is the singlet superfield. The dimensionless parameters  $\lambda$  and  $\kappa$  play roles analogous to those in the  $\mathbb{Z}_3$ -invariant NMSSM, while the bilinear mass terms  $\mu$  and  $\mu'$  and the singlet tadpole term  $\xi$  explicitly break the  $\mathbb{Z}_3$  symmetry. These  $\mathbb{Z}_3$ -breaking terms are advantageous, as they are essential for resolving the tadpole problem [88, 97] and the cosmological domain-wall problem that plagues the  $\mathbb{Z}_3$ -NMSSM [98–100]. Since one among  $\mu$ ,  $\mu'$ , and  $\xi$  may be eliminated through a shift of the  $\hat{S}$  field followed by a redefinition of the remaining parameters [101], we set  $\xi = 0$  without loss of generality. The bilinear parameters  $\mu$  and  $\mu'$  may naturally reside at the electroweak scale, originating from an underlying discrete R-symmetry  $Z_4^R$  after supersymmetry breaking [101–104].

## 2.2 Higgs Sector

The soft SUSY-breaking Lagrangian for the Higgs fields in the GNMSSM takes the form:

$$-\mathcal{L}_{soft} = \left[ \lambda A_\lambda S H_u \cdot H_d + \frac{1}{3} \kappa A_\kappa S^3 + m_3^2 H_u \cdot H_d + \frac{1}{2} m_S'^2 S^2 + \xi' S + h.c. \right] + m_{H_u}^2 |H_u|^2 + m_{H_d}^2 |H_d|^2 + m_S^2 |S|^2, \quad (2.2)$$

Here,  $H_u$ ,  $H_d$ , and  $S$  denote the scalar components of the Higgs superfields, and  $m_{H_u}^2$ ,  $m_{H_d}^2$ , and  $m_S^2$  are their soft-breaking masses. After solving the EWSB conditional equations to minimize the scalar potential and expressing these soft masses in terms of the vacuum expectation values (vevs), namely,  $\langle H_u^0 \rangle = v_u/\sqrt{2}$ ,  $\langle H_d^0 \rangle = v_d/\sqrt{2}$ , and  $\langle S \rangle = v_s/\sqrt{2}$ , with  $v = \sqrt{v_u^2 + v_d^2} \simeq 246$  GeV and  $\tan\beta \equiv v_u/v_d$ , the Higgs sector is governed by eleven independent parameters:  $\tan\beta$ ,  $v_s$ , the Yukawa couplings  $\lambda$  and  $\kappa$ , the soft-breaking trilinear coefficients  $A_\lambda$  and  $A_\kappa$ , the bilinear mass parameters  $\mu$  and  $\mu'$ , the soft-breaking parameters  $m_3^2$  and  $m_S'^2$ , and the soft-breaking tadpole coefficient  $\xi'$  that is assumed to vanish in the present analysis.

To clearly delineate the properties of the Higgs states, it is convenient to use rotated field combinations:  $H_{SM} \equiv \sqrt{2} \text{Re}(\sin\beta H_u^0 + \cos\beta H_d^0)$ ,  $H_{NSM} \equiv \sqrt{2} \text{Re}(\cos\beta H_u^0 - \sin\beta H_d^0)$ , and  $A_{NSM} \equiv \sqrt{2} \text{Im}(\cos\beta H_u^0 + \sin\beta H_d^0)$ , where  $H_{SM}$  behaves like the SM Higgs field, and  $H_{NSM}$  and  $A_{NSM}$  describing the additional doublet fields [96]. The singlet field remains unrotated and is written as  $\sqrt{2}S \equiv H_S + iA_S$ .

In the basis  $(H_{NSM}, H_{SM}, \text{Re}[S])$ , the elements of the symmetric squared mass matrix for the  $CP$ -even Higgs boson can be written in the following forms [88, 105]:

$$\begin{aligned} \mathcal{M}_{S,11}^2 &= m_A^2 + \frac{1}{2}(2m_Z^2 - \lambda^2 v^2) \sin^2 2\beta, \\ \mathcal{M}_{S,12}^2 &= -\frac{1}{4}(2m_Z^2 - \lambda^2 v^2) \sin 4\beta, \\ \mathcal{M}_{S,13}^2 &= \sqrt{2} \lambda \mu_{tot} v (\delta - 1) \cot 2\beta, \\ \mathcal{M}_{S,22}^2 &= m_Z^2 \cos^2 2\beta + \frac{1}{2} \lambda^2 v^2 \sin^2 2\beta, \\ \mathcal{M}_{S,23}^2 &= \sqrt{2} \lambda \mu_{tot} v \delta, \\ \mathcal{M}_{S,33}^2 &= m_B^2, \end{aligned} \quad (2.3)$$

while those for the  $CP$ -odd Higgs boson in the basis  $(A_{NSM}, A_S)$  are:

$$\mathcal{M}_{P,11}^2 = m_A^2, \quad \mathcal{M}_{P,22}^2 = m_C^2, \quad \mathcal{M}_{P,12}^2 = \frac{\lambda v}{\sqrt{2}} (A_\lambda - m_N). \quad (2.4)$$

We introduce a  $\delta$  factor in  $\mathcal{M}_{S,13}^2$  and  $\mathcal{M}_{S,23}^2$ , defined as:

$$\delta \equiv 1 - \frac{(A_\lambda + m_N) \sin 2\beta}{2\mu_{tot}}, \quad (2.5)$$

with the Higgsino mass  $\mu_{tot} \equiv \mu_{eff} + \mu = \lambda v_s/\sqrt{2} + \mu$  and the Singlino mass  $m_N \equiv \sqrt{2} \kappa v_s + \mu'$ , to simplify the expression and allow for direct manipulation of the mixings

of  $H_S$  with  $H_{SM}$  and  $H_{NSM}$ . This factor is expected to be tiny in the alignment without decoupling limit [34, 106].  $m_A$  is the typical definition of the mass of the doublet-like pseudoscalar Higgs field.  $m_B$  and  $m_C$  characterize the singlet-like CP-even, and the singlet-like CP-odd Higgs masses, respectively. Then the soft-breaking parameters  $A_\kappa$ ,  $m_3^2$  and  $m_S^{\prime 2}$  can be expressed in terms of the physical input parameters:

$$\begin{aligned} A_\kappa &= \frac{2m_B^2}{m_N - \mu'} + \frac{\lambda^2 v^2}{4\kappa\mu_{eff}^2} [(A_\lambda + \mu') \sin 2\beta - 2\mu] - 2m_N - \mu', \\ m_3^2 &= \frac{1}{2} [m_A^2 \sin 2\beta - \mu_{eff}(2A_\lambda + m_N + \mu')], \\ m_S^{\prime 2} &= \frac{1}{2} [m_B^2 - m_C^2 + \lambda\kappa v^2 \sin 2\beta - (m_N - \mu')(2A_\kappa + m_N + \mu')]. \end{aligned} \quad (2.6)$$

Note that the mass parameter for the singlet-like CP-odd Higgs  $m_C$  is fixed at 800 GeV in this study for simplicity to be consistent with current collider experimental limitations [8, 107].

Diagonalizing the squared mass matrix with mixing angles, denoted as  $V_{h_i}^j$ , yields three CP-even Higgs mass eigenstates:

$$h_i = V_{h_i}^{NSM} H_{NSM} + V_{h_i}^{SM} H_{SM} + V_{h_i}^S H_S, \quad (2.7)$$

with  $h_i = \{h_s, h, H\}$  ordered by ascending mass. The second CP-even mass eigenstate  $h$  corresponds to the observed 125 GeV SM-like Higgs boson. This state is predominantly composed of the  $H_{SM}$  component, requiring contributions from  $H_{NSM}$  and  $\text{Re}[S]$  components restricted to be less than about 10% [108, 109], i.e.,  $\sqrt{(V_h^{NSM})^2 + (V_h^S)^2} \lesssim 0.1$  and  $|V_h^{SM}| \sim 1$  consistent with current Higgs data. In addition, the imaginary components  $A_S$  and  $A_{NSM}$  mix into two CP-odd Higgs mass eigenstates  $a_i = \{A_H, A_s\}$ , while the charged components give rise to a pair of charged Higgs bosons  $H^\pm$ . The light CP-odd Higgs boson  $A_H$  and the charged Higgs bosons  $H^\pm$  should exhibit a nearly degenerate mass with the heavy CP-even boson  $H$ .

The present study assumes that the lightest CP-even Higgs boson  $h_s$  is singlet-dominated and fully accounts for both the  $\gamma\gamma$  and  $b\bar{b}$  excesses near 95.4 GeV. The signal strengths normalized to their SM predictions are [51]:

$$\mu_{\gamma\gamma}|_{m_{h_s}=95.4 \text{ GeV}} = \frac{\sigma_{\text{SUSY}}(pp \rightarrow h_s)}{\sigma_{\text{SM}}(pp \rightarrow h_s)} \times \frac{\text{Br}_{\text{SUSY}}(h_s \rightarrow \gamma\gamma)}{\text{Br}_{\text{SM}}(h_s \rightarrow \gamma\gamma)}, \quad (2.8)$$

$$\mu_{b\bar{b}}|_{m_{h_s}=95.4 \text{ GeV}} = \frac{\sigma_{\text{SUSY}}(e^+e^- \rightarrow Zh_s)}{\sigma_{\text{SM}}(e^+e^- \rightarrow Zh_s)} \times \frac{\text{Br}_{\text{SUSY}}(h_s \rightarrow b\bar{b})}{\text{Br}_{\text{SM}}(h_s \rightarrow b\bar{b})}, \quad (2.9)$$

where the mass of  $h_s$  is fixed at 95.4 GeV. The production rate  $\sigma(pp \rightarrow h_s)$  and the decay branching ratio  $\text{Br}(h_s \rightarrow \gamma\gamma)$  labeled with the subscript ‘SUSY’ refer to the predictions from the model, whereas those with the subscript ‘SM’ assume SM couplings for  $h_s$ .

The  $\gamma\gamma b\bar{b}$  excess near 650 GeV can be attributed to the heavy doublet-dominated CP-even Higgs boson  $H$  decaying into a SM-like Higgs boson  $h$  and a singlet-dominated Higgs boson  $h_s$ . The cross section of the resonance in the  $\gamma\gamma b\bar{b}$  channel can be expressed

as follows:

$$\sigma_{\gamma\gamma b\bar{b}} = \sigma(gg \rightarrow H) \times \text{Br}_{\text{SUSY}}(H \rightarrow hh_s) \times \text{Br}_{\text{SUSY}}(h \rightarrow \gamma\gamma) \times \text{Br}_{\text{SUSY}}(h_s \rightarrow b\bar{b}), \quad (2.10)$$

where the masses of  $H, h$  and  $h_s$  are fixed at approximately 650 GeV, 125 GeV and 95.4 GeV, respectively. By fitting the GNMSSM predictions for  $\mu_{\gamma\gamma}$ ,  $\mu_{b\bar{b}}$ , and  $\sigma_{\gamma\gamma b\bar{b}}$  to the observed experimental rates, we can investigate the viability of the GNMSSM as a unified interpretation for the 95 GeV and 650 GeV excesses.

### 2.3 Neutralino Sector

The neutralino sector within the GNMSSM framework is comprised of five superpartners: the gaugino fields ( $\tilde{B}$ , the Bino, and  $\tilde{W}$ , the Wino), the Higgsino fields ( $\tilde{H}_d^0$  and  $\tilde{H}_u^0$ ), and the Singlino field ( $\tilde{S}$ ). In the basis  $\psi^T \equiv (\tilde{B}, \tilde{W}, \tilde{H}_d^0, \tilde{H}_u^0, \tilde{S})$ , the symmetric  $5 \times 5$  neutralino mass matrix,  $\mathcal{M}$ , is given by [88]:

$$\mathcal{M} = \begin{pmatrix} M_1 & 0 & -m_Z \sin \theta_W \cos \beta & m_Z \sin \theta_W \sin \beta & 0 \\ M_2 & m_Z \cos \theta_W \cos \beta & -m_Z \cos \theta_W \sin \beta & 0 & 0 \\ 0 & 0 & -\mu_{tot} & -\frac{1}{\sqrt{2}} \lambda v \sin \beta & 0 \\ 0 & 0 & 0 & -\frac{1}{\sqrt{2}} \lambda v \cos \beta & 0 \\ 0 & 0 & 0 & 0 & m_N \end{pmatrix}, \quad (2.11)$$

where  $\theta_W$  is the weak mixing angle, and  $M_1$  and  $M_2$  are the soft-breaking masses of the Bino and Wino, respectively. Diagonalizing  $\mathcal{M}$  by a rotation matrix  $N$  yields five neutralino mass eigenstates:

$$\tilde{\chi}_i^0 = \sum_{j=1}^5 N_{ij} \psi_j^0, \quad i = 1, \dots, 5, \quad (2.12)$$

ordered by increasing mass. The element  $N_{ij}$  parametrizes the contribution of the interaction eigenstate  $\psi_j^0$  to the physical neutralino  $\tilde{\chi}_i^0$ . Under  $R$  parity conservation, the lightest neutralino  $\tilde{\chi}_1^0$  is stable and constitutes a viable DM candidate when it is the Lightest Supersymmetric Particle (LSP). In many NMSSM realizations, a Singlino-dominated LSP naturally reproduces the observed relic abundance while evading stringent direct detection bounds [110]. In the present study, however, this possibility is strongly limited. The relatively large value of  $\lambda$  required to account for both the excesses enhances the Higgs-mediated scattering cross section of a Singlino-like LSP, bringing it into tension with current direct detection limits [93, 111]. Furthermore, the mixing constraints on  $V_{h_i}^{\text{SM}}$  and  $V_{h_i}^{\text{NSM}}$  required by the 95 GeV and 650 GeV anomalies further reduce the viable parameter space for Singlino-like DM. In contrast, as will be demonstrated later, the combined interpretation of the excesses instead favors a Bino-dominated LSP. Such a Bino-like neutralino can efficiently reduce its relic abundance through Higgs-funnel annihilation and/or coannihilations with Singlino-, Higgsino-, or Wino-like electroweakinos. The spin-independent (SI) and spin-dependent (SD)  $\tilde{\chi}_1^0$ -nucleon scattering cross-sections depend on the  $\tilde{\chi}_1^0$  couplings to the Higgs boson and the  $Z$  gauge boson, respectively. Both can be heavily suppressed due to cancellations among different contributions or by the emergence of blind-spot conditions [112–121].

### 3 Explanation of the excesses

This section outlines the parameter-sampling strategy and presents detailed numerical results that account for the observed excesses in the diphoton and  $b\bar{b}$  final states—both separately and simultaneously—while remaining consistent with other experimental constraints, in particular those from Higgs data and DM detections. The numerical procedure follows several steps. First, we implement the GNMSSM using SARAH-4.14.3 [122–125] to generate analytical model files. Second, the packages SPheno-4.0.5 [126, 127] and FlavorKit [128] are used to compute the SUSY mass spectrum and low-energy flavor observables, respectively. Subsequently, DM observables—including relic density, annihilation channels, and direct detection rates—are evaluated with MicrOMEGAs-5.0.4 [129–138]. Finally, the resulting samples are then analyzed using both Bayesian and Frequentist statistical frameworks: the posterior probability density function (PDF) and the profile likelihood (PL) [139]. These complementary approaches provide a robust characterization of the viable parameter space and enable a nuanced interpretation of the experimental anomalies.

#### 3.1 Strategy in scanning the parameter space

To thoroughly investigate the phenomenological implications of the observed excesses and DM constraints, we employ a sophisticated scan strategy focusing on phenomenologically relevant input parameters. The scan includes all parameters relevant to the Higgs sector. However, instead of directly scanning the original soft-breaking parameters ( $m_{\tilde{2}}^2, A_\kappa, A_\lambda$ ) appearing in Eq. (2.2), we trade them for the physical and semi-physical masses and mixing terms ( $m_A, m_B$ , and  $\delta$ ) as defined in Eqs. (2.6) and (2.5). This substitution improves the efficiency of the sampling by allowing direct exploration of regions consistent with a target Higgs mass spectrum while preserving the essential physics. The soft trilinear couplings of the third-generation squarks,  $A_t$  and  $A_b$ , are treated as free parameters because of their crucial impact on the radiative corrections to the SM-like Higgs mass. Furthermore, the soft gaugino masses  $M_1$  and  $M_2$  are included as scan parameters to allow for a Bino-dominated  $\tilde{\chi}_1^0$  DM candidate, as suggested by the analysis in Sec. 2. In total, the scan explores a 12-dimensional parameter space as delineated in Table. 1. The parameter ranges are carefully determined based on theoretical considerations and exploratory trial scans across broader intervals to ensure both comprehensive coverage and effective exploration of the regions of interest. All final samples are required to respect the constraint of field-theoretic perturbativity between the electroweak and GUT scales. The approximate bound derived for the  $\mathbb{Z}_3$ -NMSSM [105],  $\lambda^2 + \kappa^2 \lesssim 0.5$ , is applied here, as the GNMSSM beta functions do not introduce new scale-dependent contributions up to the two-loop level (see Appendices in Refs. [88, 140, 141]). All numerical results presented in this work are ensured to satisfy this condition.

The multi-dimensional parameter space is explored using the MultiNest algorithm [142, 143], a highly efficient nested sampling method, with a fixed number of live points set to  $n_{live} = 6000$  to ensure comprehensive survey and accurate computation of the Bayesian evidence and posterior distributions<sup>1</sup>. The likelihood function guiding the scan is

---

<sup>1</sup>In nested sampling algorithms,  $n_{live}$  denotes the number of active (live) points used to define successive

**Table 1.** Ranges of input parameters used in this study. All parameters are assigned flat priors due to their well-defined physical interpretation. The soft trilinear coefficients for third-generation squarks are unified as  $A_t = A_b$ . Dimensional parameters not directly relevant here are fixed to simplify the analysis and comply with experimental constraints: the gluino mass is set to  $M_3 = 3$  TeV, and other unspecified parameters are fixed at 2 TeV to satisfy LHC limits on SUSY particles. All parameters are defined at the renormalization scale  $Q_{\text{input}} = 1$  TeV.

Parameter	Prior	Range	Parameter	Prior	Range
$\lambda$	Flat	0.5 $\sim$ 0.7	$\mu_{\text{tot}}/\text{GeV}$	Flat	500.0 $\sim$ 1000
$\kappa$	Flat	-0.5 $\sim$ 0.5	$\mu_{\text{eff}}/\text{GeV}$	Flat	-1000 $\sim$ 1000
$\delta$	Flat	-0.05 $\sim$ 0.05	$m_A/\text{GeV}$	Flat	500.0 $\sim$ 650.0
$\tan\beta$	Flat	1.0 $\sim$ 2.0	$m_B/\text{GeV}$	Flat	90.0 $\sim$ 120
$M_1/\text{GeV}$	Flat	-1000 $\sim$ -200.0	$A_t/\text{GeV}$	Flat	1000 $\sim$ 3000
$M_2/\text{GeV}$	Flat	200.0 $\sim$ 1000	$m_N/\text{TeV}$	Flat	-1000 $\sim$ 1000

constructed as  $\mathcal{L} \equiv \mathcal{L}_{650+95} \times \mathcal{L}_{\text{Res}}$ . The first factor  $\mathcal{L}_{650+95} = \exp(-\frac{1}{2}\chi_{650+95}^2)$  quantifies the compatibility of the GNMSSM predictions with the central values and uncertainties of the experimental observations of the  $\gamma\gamma$  plus  $b\bar{b}$  excesses near 650GeV and the 95GeV diphoton and  $b\bar{b}$  excesses, via a  $\chi^2$  function:

$$\chi_{650+95}^2 = \left( \frac{\sigma_{\gamma\gamma b\bar{b}} - 0.35 \text{ fb}}{0.13 \text{ fb}} \right)^2 + \left( \frac{\mu_{\gamma\gamma} - 0.24}{0.08} \right)^2 + \left( \frac{\mu_{b\bar{b}} - 0.117}{0.057} \right)^2. \quad (3.1)$$

The second factor,  $\mathcal{L}_{\text{Res}}$  term enforces essential physical and experimental bounds by acting as a step function:  $\mathcal{L}_{\text{Res}} = 1$  if all conditions are met, and  $\mathcal{L}_{\text{Res}} = \exp[-100]$  otherwise. The required restrictions include:

- **Masses of the three scalars:** To interpret the observed excesses, we impose specific mass requirements on the three  $CP$ -even Higgs bosons:
  - Light Scalar ( $h_s$ ): The mass of the light scalar boson is required to be in the range  $95.4 \pm 1$  GeV to align with experimental hints. This choice is motivated by the fact that a singlet-like boson typically receives smaller radiative corrections than the SM-like Higgs.
  - Heavy Resonance ( $H$ ): The heavy scalar mass is constrained to the range  $650 \pm 25$  GeV to match the resonant excess observed by CMS [10, 11].
  - SM-like Higgs ( $h$ ): The mass of the SM-like Higgs boson must be consistent with the LHC measurements, allowing for a  $\pm 3$  GeV tolerance to account for combined experimental and theoretical uncertainties.
- **SM-like Higgs data fit:** The SM-like Higgs boson must satisfy the ATLAS and CMS measurements at the 95% confidence level. This condition is validated using the newest version of the HiggsTools code that incorporates the HiggsSignals-2 [144–147], which compares model predictions to a full set of current measurements of the

---

iso-likelihood contours [142, 143]. Larger values of *nlive* improve the resolution of the parameter space at the cost of increased computational time.

125GeV Higgs properties and returns a  $\chi^2$  value that quantifies the agreement of the model predictions with the measurements. The  $\chi^2$  value is directly incorporated into the likelihood function. When presenting results in two-dimensional parameter planes, samples satisfying  $\Delta\chi_{125}^2 \equiv \chi^2 - \chi_{125,\text{SM}}^2 \lesssim 6.18$ , where  $\chi_{125,\text{SM}}^2 = 153$  denotes the SM best-fit value, are considered consistent with the Higgs data at approximately the  $2\sigma$  confidence level (assuming Gaussian uncertainties) [148].

- **Extra Higgs searches:** Signal rates for all non-SM Higgs bosons ( $h_s, H, A_H, H^\pm$ ) must comply with cross-section limits based on experimental data at LEP, Tevatron, and the LHC. This requirement is implemented using the `HiggsTools` code [149] with the complete `HiggsBounds-5.10.2` library [150–154].
- **DM relic density:** The predicted DM relic density must agree with the Planck-2018 central value ( $\Omega h^2 = 0.120$ ) [155], allowing for a conservative 20% theoretical uncertainty:  $0.096 \leq \Omega h^2 \leq 0.144$ .
- **DM detections:** The SI and SD  $\tilde{\chi}_1^0$ -nucleon scattering cross-sections must be below the currently most stringent upper bounds imposed by the LZ experiments [156, 157]. Constraints from DM indirect searches are not considered here as they are less restrictive for the masses under consideration ( $|m_{\tilde{\chi}_1^0}| \gtrsim 100$  GeV) [158].
- **$B$ -physics observables:** The branching ratios  $B_s \rightarrow \mu^+\mu^-$  and  $B \rightarrow X_s\gamma$  are required to agree with current experimental measurements at the  $2\sigma$  level [159].
- **Vacuum stability:** The electroweak vacuum must be demonstrated to be either the global minimum or a sufficiently long-lived, metastable vacuum state [160]. This is rigorously tested using the `VevaciousPlusPlus` code [161, 162].

Constraints from LHC searches for electroweakinos are expected to have a negligible impact on the scan results. This is because the gaugino–Higgsino states in Table. 1 lie in relatively heavy mass ranges, and all other SUSY particles are assumed to be heavy and decoupled. This estimation is consistent with recent statistical combinations of ATLAS Run 2 searches [163]. To confirm this, we evaluate all sampled points using `SModelS-3.0.0`, which implements a wide set of simplified-model constraints by decomposing SUSY signatures into experimentally tested topologies and applying the corresponding efficiency maps [164]. Furthermore, four representative benchmark points are subjected to dedicated Monte Carlo simulations. For each benchmark,  $10^6$  events were generated with `MadGraph_aMC@NLO` [165, 166] for the following electroweakino production channels:

$$\begin{aligned}
pp &\rightarrow \tilde{\chi}_i^0 \tilde{\chi}_j^\pm, & i = 2, 3, 4, 5; & \quad j = 1, 2 \\
pp &\rightarrow \tilde{\chi}_i^\pm \tilde{\chi}_j^\mp, & i, j = 1, 2; \\
pp &\rightarrow \tilde{\chi}_i^0 \tilde{\chi}_j^0, & i, j = 2, 3, 4, 5.
\end{aligned}
\tag{3.2}$$

Production cross sections are computed at next-to-leading order using `Prospino2` [167]. Parton showering and hadronization are performed with `PYTHIA8` [168], and detector effects

are simulated using `Delphes` [169]. The resulting events are analyzed with `CheckMATE-2.0.26` [170–172], which computes the  $R$  value, defined as the exclusion ratio  $R \equiv \max\{S_i/S_{i,obs}^{95}\}$ , with  $S_i$  representing the simulated event number of the  $i$ -th signal region (SR), and  $S_{i,obs}^{95}$  the corresponding 95% confidence level upper limit. Values of  $R > 1$  indicates exclusion (neglecting theoretical and experimental uncertainties) [173], while  $R < 1$  denotes consistency with current experimental analyses. The specific ATLAS and CMS analyses used in this study are listed in Table. A1 in the Appendix.

### 3.2 Numerical Results

The scan process yields over 25,000 parameter samples that satisfy all applied theoretical and experimental constraints. A key result across all viable samples is the preference for the Bino-dominated  $\tilde{\chi}_1^0$  as the DM candidate. These samples naturally cluster into two distinct scenarios according to the dominant mechanism responsible for achieving the observed relic abundance.:

- **Scenario I** ( $\approx 92\%$ ): Achieves the correct relic density primarily via  $A_s$  funnel annihilation or coannihilation with  $\tilde{S}$ -like  $\tilde{\chi}_2^0$ s, typically into the  $h_s A_H$  final state.
- **Scenario II** ( $\approx 8\%$ ): Achieves the correct relic density through coannihilation with  $\tilde{H}$ -like  $\tilde{\chi}_2^0$ s or  $\tilde{\chi}_1^\pm$ s, favoring the  $h_s A_s$  final state.

The correlation between the cross section  $\sigma(gg \rightarrow H \rightarrow hh_s \rightarrow \gamma\gamma b\bar{b})$  and the signal strengths  $\mu_{\gamma\gamma}$  and  $\mu_{b\bar{b}}$  are depicted in the left and right panels in Fig. 1, respectively. The orange dashed lines and shaded bands mark the central value of the cross section  $\sigma_{\gamma\gamma b\bar{b}}$  with the corresponding  $2\sigma$  uncertainty, and the blue ones mark that of the signal strengths  $\mu_{\gamma\gamma}$  and  $\mu_{b\bar{b}}$ . The purple dashed-dotted contour delineate the combined  $2\sigma$  region on each plane. The plot shows that **Scenario I** can interpret the  $\sigma_{\gamma\gamma b\bar{b}}$  excess near 650 GeV and  $\mu_{\gamma\gamma}$  and  $\mu_{b\bar{b}}$  excesses near 95 GeV at the  $2\sigma$  level at the same time. While samples in **Scenario I** can push the cross section  $\sigma(gg \rightarrow H \rightarrow hh_s \rightarrow \gamma\gamma b\bar{b})$  value closer to the  $1\sigma$  range from below, this comes at the cost of shifting  $\mu_{\gamma\gamma}$  away from the  $2\sigma$  range. Moreover, these points tend to be excluded by the CMS upper 95% CL limit of approximately 0.1 fb from the  $\tau\bar{\tau}$  plus  $b\bar{b}$  search [11, 12]. In contrast,  $\sigma(gg \rightarrow H \rightarrow hh_s \rightarrow \gamma\gamma b\bar{b})$  in **Scenario II** can reach at most 0.08 fb. Nevertheless, it achieves an overall  $2\sigma$  fit when combining the  $\sigma_{\gamma\gamma b\bar{b}}$  and  $\mu_{\gamma\gamma}$  excess, i.e.,  $\chi_{\sigma_{\gamma\gamma b\bar{b}}}^2 + \chi_{\mu_{\gamma\gamma}}^2 \leq 6.18$ . In this scenario,  $\mu_{\gamma\gamma}$  can reach its central value, whereas  $\mu_{b\bar{b}}$  remains below 0.02, though still within the  $2\sigma$  region. This behavior arises because a suppression of  $\text{Br}_{\text{SUSY}}(h_s \rightarrow b\bar{b})$  is needed to enhance the branching ratio  $\text{Br}_{\text{SUSY}}(h_s \rightarrow \gamma\gamma)$  and thus a larger  $\mu_{\gamma\gamma}$ . This also explains the trend seen in the left panel in Fig. 1, where  $\sigma(gg \rightarrow H \rightarrow hh_s \rightarrow \gamma\gamma b\bar{b})$  decreases with  $\mu_{\gamma\gamma}$  increases. Samples excluded by constraints from the Higgs experiments, DM relic density and direct detections are denoted by grey dots. In particular, the searches for additional Higgs states implemented in `HiggsBounds` set the strongest limits for  $\sigma(gg \rightarrow H \rightarrow hh_s \rightarrow \gamma\gamma b\bar{b}) \gtrsim 0.09$  fb, while the SM-like Higgs precision data encoded in `HiggsSignals` dominate the exclusions below this threshold. Furthermore, roughly half of the remaining samples are removed by DM relic density and direct detection constraints.

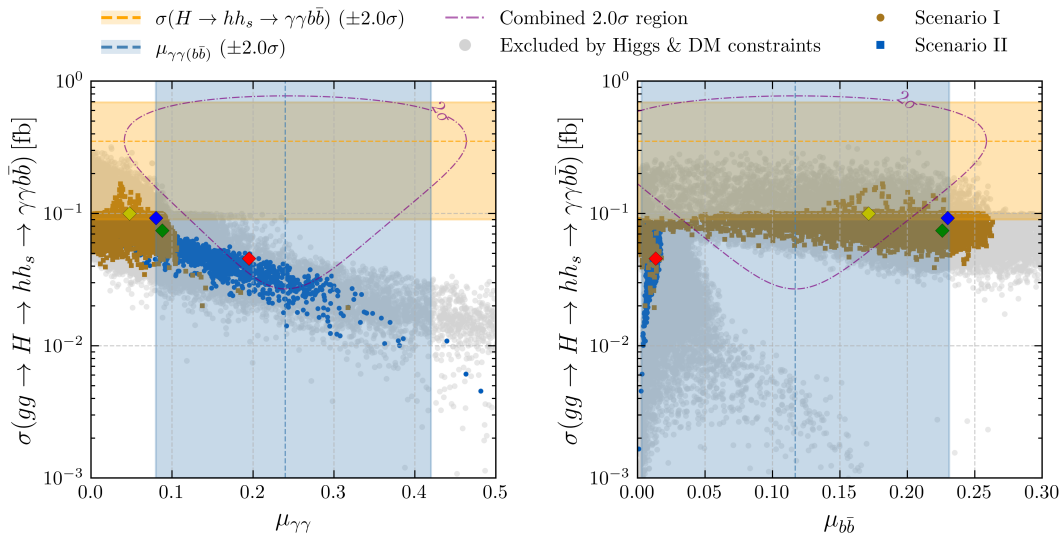


**Figure 1.** Scattering plots of samples satisfying all applied constraints, projected onto the planes of the cross section  $\sigma(gg \rightarrow H \rightarrow hh_s \rightarrow \gamma\gamma b\bar{b})$  versus the signal strengths  $\mu_{\gamma\gamma}$  (left) and  $\mu_{b\bar{b}}$  (right). The orange dashed lines and shaded bands indicate the central value of  $\sigma(gg \rightarrow H \rightarrow hh_s \rightarrow \gamma\gamma b\bar{b})$  in Eq. (1.3) with the corresponding  $2\sigma$  uncertainty, while the blue lines show the central values of  $\mu_{\gamma\gamma}$  in Eq. (1.2) (left) and  $\mu_{b\bar{b}}$  in Eq. (1.1) (right). The purple dash-dotted contours mark the combined  $2\sigma$  regions on each plane. Grey dots represent samples excluded by HiggsSignals, HiggsBounds, or by DM relic density and direct detection constraints. Amber squares and blue dots denote **Scenario I** and **Scenario II**, respectively. Colored diamonds correspond to the four benchmark points, with details listed in Table. 2 and Table. 3.

The right panel of Fig.1 displays a nontrivial correlation between  $\sigma(gg \rightarrow H \rightarrow hh_s \rightarrow \gamma\gamma b\bar{b})$  and  $\mu_{b\bar{b}}$ . This complexity arises because an increase  $\text{Br}_{\text{SUSY}}(h_s \rightarrow b\bar{b})$  does not necessarily translate into a corresponding enhancement of  $\mu_{b\bar{b}}$ . In particular, increasing the coupling of  $h_s$  to bottom quark pairs  $|C_{h_s b\bar{b}}|$  may simultaneously suppress its couplings to the electroweak gauge bosons  $|C_{h_s VV}|$ <sup>2</sup>. Because  $\mu_{b\bar{b}}$  depends not only on  $\text{Br}_{\text{SUSY}}(h_s \rightarrow b\bar{b})$  but also on the associated suppression of the  $h_s$ - $Z$  coupling,  $\mu_{b\bar{b}}$  may saturate or even decrease as  $\text{Br}_{\text{SUSY}}(h_s \rightarrow b\bar{b})$  grows. Although in most of the parameter space  $|C_{h_s b\bar{b}}|$  and  $|C_{h_s VV}|$  increase together, the associated reduction of the SM-like Higgs coupling to photons suppresses  $\text{Br}_{\text{SUSY}}(h \rightarrow \gamma\gamma)$ . This effect offsets the enhancement of  $\sigma(gg \rightarrow H \rightarrow hh_s \rightarrow \gamma\gamma b\bar{b})$  expected from increasing  $\text{Br}_{\text{SUSY}}(h_s \rightarrow b\bar{b})$ , thereby further contributing to the intricate structure in the  $\mu_{b\bar{b}}$ - $\sigma(gg \rightarrow H \rightarrow hh_s \rightarrow \gamma\gamma b\bar{b})$  correlation.

Next, we apply the Bayesian inference method to analyze the model predictions for the heavy Higgs boson  $H$  near 650 GeV. By accumulating the posterior PDF of samples

<sup>2</sup>Recalling the normalized couplings of  $h_i$  to  $b\bar{b}$  and vector bosons  $V = W, Z$  at tree level in terms of the mixing coefficients  $V_{h_i}^j$  in Eq.(2.7) :

$$C_{h_i b\bar{b}} = V_{h_i}^{\text{SM}} - V_{h_i}^{\text{NSM}} \tan \beta, \quad C_{h_i VV} = V_{h_i}^{\text{SM}},$$

$C_{h_s VV}$  may decrease with  $C_{h_s b\bar{b}}$  increases when  $V_{h_s}^{\text{SM}}$  and  $V_{h_s}^{\text{NSM}}$  share the same sign. In this study, we verify that this behaviour occurs for  $0.0 \lesssim C_{h_s b\bar{b}} \lesssim 0.3$ . Furthermore, the effective coupling of the SM-like Higgs  $h$  to  $\gamma\gamma$  decreases from about 1.0 to 0.89 once  $C_{h_s b\bar{b}} \gtrsim 0.3$ .

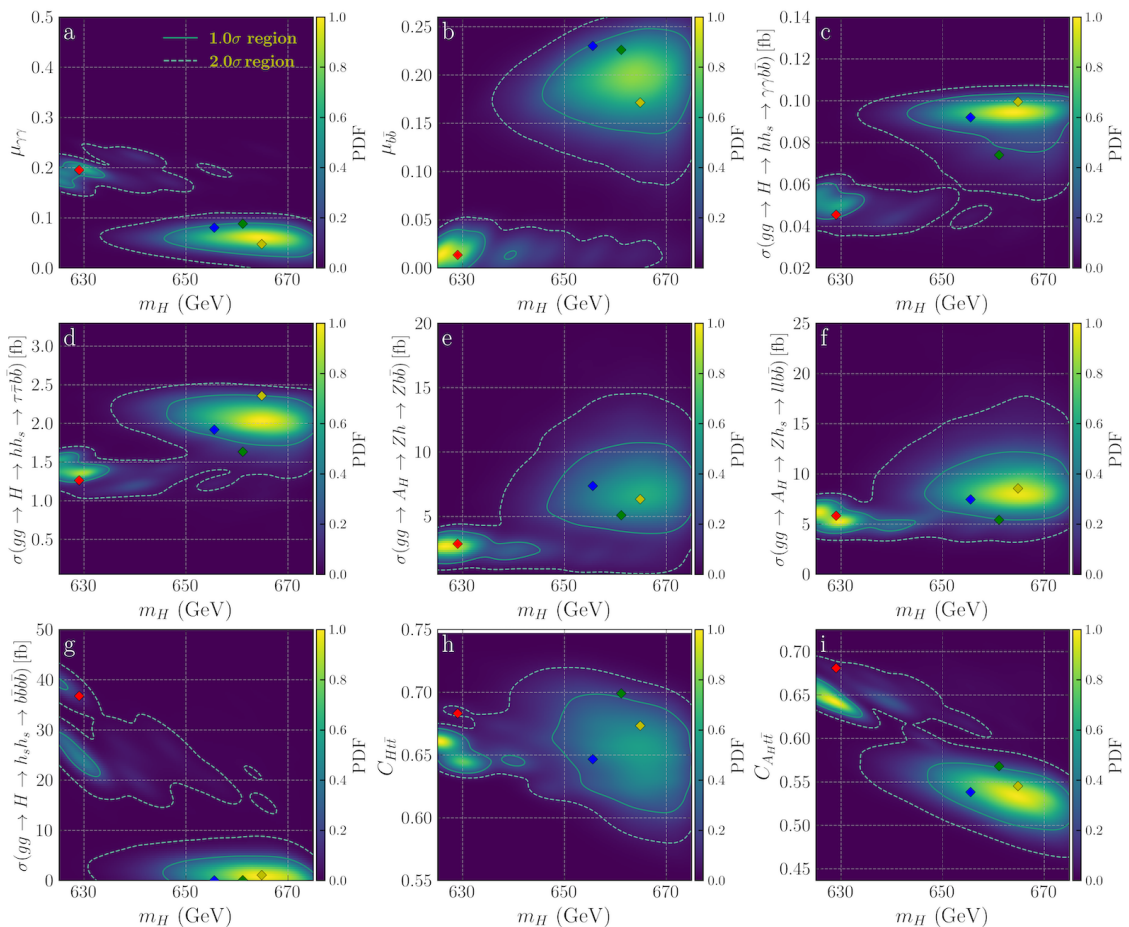


**Figure 2.** Two-dimensional posterior PDF distributions of the heavy Higgs boson mass  $m_H$  versus (a)  $\mu_{\gamma\gamma}$ , (b)  $\mu_{b\bar{b}}$ , (c)  $\sigma(gg \rightarrow H \rightarrow hh_s \rightarrow \gamma\gamma b\bar{b})$ , (d)  $\sigma(gg \rightarrow H \rightarrow hh_s \rightarrow \tau\tau b\bar{b})$ , (e)  $\sigma(gg \rightarrow A_H \rightarrow Zh \rightarrow Zb\bar{b})$ , (f)  $\sigma(gg \rightarrow A_H \rightarrow Zh_s \rightarrow \ell\ell b\bar{b})$ , (g)  $\sigma(gg \rightarrow H \rightarrow h_s h_s \rightarrow b\bar{b}b\bar{b})$ , (h)  $C_{Ht\bar{t}}$ , and (i)  $C_{A_H t\bar{t}}$ . Solid and dashed contours indicate the  $1\sigma$  and  $2\sigma$  credible regions, respectively. Colored diamonds denote the four benchmark points corresponding to those in Fig. 1, with details provided in Table. 2 and Table. 3.

obtained from the scan process<sup>3</sup>, we find that **Scenario I** and **Scenario II** contribute approximately 68% and 23% of the total Bayesian evidence, respectively, indicating a clear preference of current experimental data for the former. The posterior PDF distributions of  $\mu_{\gamma\gamma}$ ,  $\mu_{b\bar{b}}$ , and  $\sigma(gg \rightarrow H \rightarrow hh_s \rightarrow \gamma\gamma b\bar{b})$  as functions of the heavy Higgs mass  $m_H$  are shown in the upper panels of Fig. 2. The solid contours indicate the  $1\sigma$  credible regions.

<sup>3</sup>The nested sampling algorithm used in this work transforms the multidimensional evidence integral into a one-dimensional integral while sampling the parameter space [142, 143, 174, 175]. The evidence integral can be written as [142]:

$$\mathcal{Z} = \int_0^1 \mathcal{L}(X) dX, \quad X(\lambda) = \int_{\mathcal{L}(\Theta)} \pi(\Theta) d^D \Theta,$$

where  $\Theta$  is the input parameters of the model,  $D$  the dimensionality of the parameter space,  $\pi(\Theta)$  the prior,  $\mathcal{L}(\Theta)$  the likelihood, and  $X$  the ‘prior volume’ with the definition  $dX = \pi(\Theta) d^D \Theta$ .

For  $625 \text{ GeV} \lesssim m_H \lesssim 640 \text{ GeV}$ , we find:

$$0.16 \lesssim \mu_{\gamma\gamma} \lesssim 0.21, \quad 0.0 \lesssim \mu_{b\bar{b}} \lesssim 0.04, \quad 0.04 \text{ fb} \lesssim \sigma(gg \rightarrow H \rightarrow hh_s \rightarrow \gamma\gamma b\bar{b}) \lesssim 0.06 \text{ fb}.$$

For  $640 \text{ GeV} \lesssim m_H \lesssim 675 \text{ GeV}$ , we find:

$$0.02 \lesssim \mu_{\gamma\gamma} \lesssim 0.09, \quad 0.14 \lesssim \mu_{b\bar{b}} \lesssim 0.25, \quad 0.07 \text{ fb} \lesssim \sigma(gg \rightarrow H \rightarrow hh_s \rightarrow \gamma\gamma b\bar{b}) \lesssim 0.105 \text{ fb}.$$

As expected, **Scenario I** and **Scenario II** primarily populate the regions with  $m_H \lesssim 640 \text{ GeV}$  and  $m_H \gtrsim 640 \text{ GeV}$ , respectively. The pattern displayed in the  $\mu_{\gamma\gamma} - m_H$  and  $\mu_{b\bar{b}} - m_H$  planes can be understood from the fact that heavier mass of  $m_H$  requires an increasing  $\text{Br}_{\text{SUSY}}(h_s \rightarrow b\bar{b})$  to keep  $\sigma(gg \rightarrow H \rightarrow hh_s \rightarrow \gamma\gamma b\bar{b})$  from decreasing for kinematic reasons, thus leading to a higher  $\mu_{b\bar{b}}$  and lower  $\mu_{\gamma\gamma}$ .

As mentioned earlier, the cross section  $\sigma(gg \rightarrow H \rightarrow hh_s \rightarrow \tau\tau b\bar{b})$  is constrained to be below about 3 fb for  $600 \text{ GeV} \lesssim m_H \lesssim 700 \text{ GeV}$  by CMS [12]. Panel (d) of Fig. 2 shows that both the  $1\sigma$  and  $2\sigma$  credible regions lie well within the current experimental bounds.

We further explore several phenomenologically interesting search channels and present their prospects as tests of the model. The scenarios studied here predict a doublet-like CP-odd Higgs boson  $A_H$  with a mass range of  $450 \text{ GeV} \lesssim m_{A_H} \lesssim 650 \text{ GeV}$  (corresponding to  $m_H$  varying from  $\sim 675 \text{ GeV}$  to  $\sim 625 \text{ GeV}$ ) at the  $1\sigma$  level. Searches in the channel  $\sigma(gg \rightarrow A_H \rightarrow Zh \rightarrow Zb\bar{b})$  conducted by CMS [176] and ATLAS [177] place a 95% CL upper limit of roughly 30 fb near  $m_{A_H} \simeq 600 \text{ GeV}$  (or equivalently  $m_H \simeq 645 \text{ GeV}$ ). This limit relaxes to about 100 fb as  $m_{A_H}$  decreases to 450 GeV (or  $m_H$  increases to 675 GeV). Searches in the complementary channel  $\sigma(gg \rightarrow A_H \rightarrow Zh_s \rightarrow \ell\ell b\bar{b})$  by CMS [178] impose upper limits between 20 and 30 fb for  $625 \text{ GeV} \lesssim m_H \lesssim 675 \text{ GeV}$ . Panels (e) and (f) of Fig. 2 display the corresponding predictions, demonstrating that they lie safely below the current bounds and are likely to be probed at future high-luminosity collider runs.

Considering that the decays of  $H$  or  $A_H$  into top-quark pairs may provide promising search channels, we show the normalized couplings  $C_{Ht\bar{t}}$  and  $C_{A_H t\bar{t}}$  in panels (h) and (i) of Fig. 2, respectively. The CMS search for heavy resonances decaying into  $t\bar{t}$  [179] sets an approximate upper limit of  $C_{Ht\bar{t}} \simeq 0.86$  for the ratio of width to mass  $\Gamma_H/m_H \simeq 2.5\%$ , and  $C_{A_H t\bar{t}} \simeq 0.75$  for  $\Gamma_{A_H}/m_{A_H} \simeq 2.5\%$  with  $m_H \simeq 629 \text{ GeV}$ . It is worth noting that in panel (i) of Fig. 2 the region with  $C_{A_H t\bar{t}} \lesssim 0.60$  corresponds entirely to **Scenario I**, while values above 0.6 correspond to **Scenario II**. The origin of this separation is clarified later in the discussion of the lower-left panel of Fig. 3.

We also calculate the cross sections of  $H$  decaying into the SM-like Higgs pairs  $\sigma(gg \rightarrow H \rightarrow hh)$  and the light Higgs pairs  $\sigma(gg \rightarrow H \rightarrow h_s h_s)$ . The largest value in the  $1\sigma$  region of  $\sigma(gg \rightarrow H \rightarrow hh)$  is about 20 fb for **Scenario I** and 3.5 fb for **Scenario II**. For the  $h_s h_s$  channel, this channel is significantly more promising, with the largest cross-section reaching 25 fb for **Scenario I** and a substantial 120 fb for **Scenario II**. The largest predicted values of  $\sigma(gg \rightarrow H \rightarrow h_s h_s)$  multiplied by the relevant branching fractions into the final states  $b\bar{b}b\bar{b}$ ,  $b\bar{b}\tau\bar{\tau}$ , and  $b\bar{b}\gamma\gamma$  are approximately 36 fb, 4.5 fb and 0.23 fb, respectively. The distribution of the  $\sigma(gg \rightarrow H \rightarrow h_s h_s \rightarrow b\bar{b}b\bar{b})$  cross-section is displayed in panel (g) of Fig. 2.

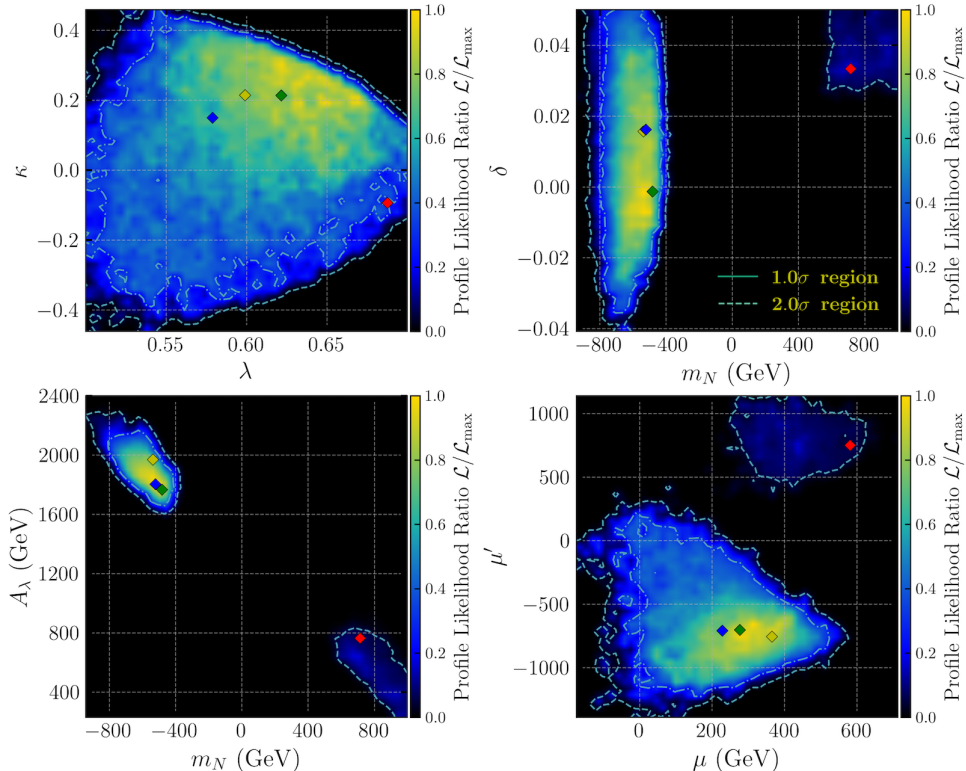


**Figure 3.** Two-dimensional profile likelihoods projected onto the  $(\lambda, \kappa)$ ,  $(m_N, \delta)$ ,  $(m_N, A_\lambda)$ , and  $(\mu, \mu')$  planes. Dashed-dotted and dashed contours indicate the  $1\sigma$  and  $2\sigma$  confidence intervals, respectively. The best-fit point has a total  $\chi^2$  value of  $\chi_{650+95}^2 + \chi_{125}^2 \simeq 162$ . Colored diamonds denote the four benchmark points shown in Figs. 1 and 2.

Fig. 3 shows the two-dimensional PL functions projected onto the  $(\lambda, \kappa)$ ,  $(m_N, \delta)$ ,  $(m_N, A_\lambda)$  and  $(\mu, \mu')$  planes<sup>4</sup>. The dashed-dotted and dashed contours delineate the  $1\sigma$  and  $2\sigma$  confidence intervals, respectively. The best-fit point yields a combined value of  $\chi_{650+95}^2 + \chi_{125}^2 \simeq 162$ . The upper-left panel shows that the  $1\sigma$  regions of  $\lambda$  and  $\kappa$  span nearly the entire prior range, bounded only by the perturbativity condition. The preferred region lies at relatively large and positive values of  $(\lambda, \kappa)$ , where **Scenario I** and **Scenario II** overlap. In contrast, the remaining three panels reveal two clearly separated islands of viable solutions. We verify that

$$\textbf{Scenario I} : m_N \lesssim -390 \text{ GeV}, \quad A_\lambda \gtrsim 1600 \text{ GeV}, \quad \mu' \lesssim 400 \text{ GeV},$$

while

$$\textbf{Scenario II} : m_N \gtrsim 550 \text{ GeV}, \quad A_\lambda \lesssim 800 \text{ GeV}, \quad \mu' \gtrsim 500 \text{ GeV},$$

<sup>4</sup>The two-dimensional profile likelihood for parameters  $(\theta_1, \theta_2)$  is defined as

$$\mathcal{L}_{\text{prof}}(\theta_1, \theta_2) = \max_{\theta_3, \dots, \theta_n} \mathcal{L}(\theta_1, \theta_2, \theta_3, \dots, \theta_n).$$

At each point in the  $(\theta_1, \theta_2)$  plane, it represents the maximum likelihood compatible with the data after optimizing over all remaining nuisance parameters. The profile likelihood therefore encodes the maximally allowed parameter region consistent with current experimental data

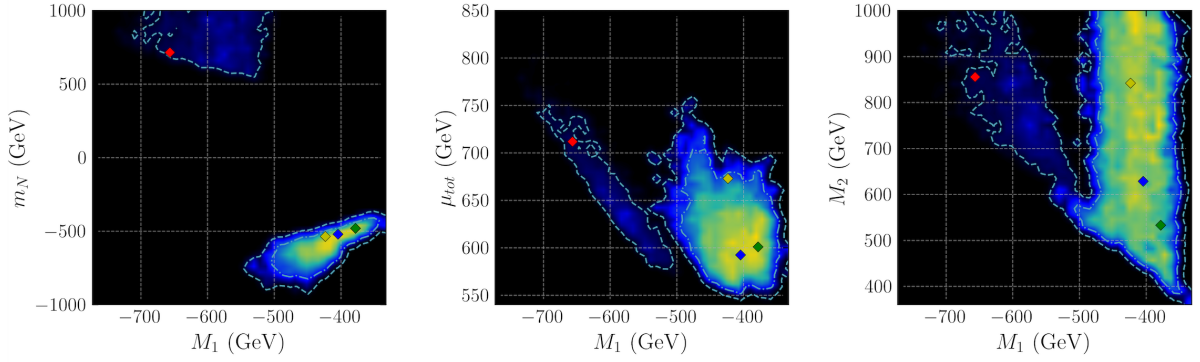


**Figure 4.** Same as Fig. 3, but projected onto  $(M_1, m_N)$ ,  $(M_1, \mu_{tot})$ ,  $(M_1, M_2)$  planes.

corresponding only to the  $2\sigma$  credible region.

The structure seen in the lower-left panel of Fig. 3 indicates that  $A_\lambda + m_N$  is confined to nearly the same range in both scenarios. This behavior follows from the requirement that  $A_\lambda + m_N \simeq 2\mu_{tot}$  (given  $\tan\beta \simeq 1.6$ ), which is necessary to keep  $\delta$  in the small range demanded by Eq. (2.5). Moreover, in **Scenario I**, the enhancement of  $A_\lambda - m_N$  leads to a relatively larger mixing between  $A_{NSM}$  and  $A_S$  [see Eq. (2.4)], thereby suppressing the coupling of  $A_H$  to top-quark pairs. Conversely, in **Scenario II**, the partial cancellation between  $A_\lambda$  and  $m_N$  yields a larger  $C_{A_H t\bar{t}}$ , consistent with the pattern shown in panel (i) of Fig. 2. Finally, the  $(\mu, \mu')$  panel reveals  $1\sigma$  and  $2\sigma$  regions that significantly deviate from zero, suggesting that non-vanishing values of  $\mu$  and  $\mu'$  may serve as distinguishing features of the GNMSSM relative to the  $\mathbb{Z}_3$ -NMSSM and the MSSM.

Lastly, we discuss the DM dynamics relevant for explaining the observed excesses. Since both scenarios predict a Bino-dominated neutralino  $\tilde{\chi}_1^0$  as the DM candidate, we show in Fig. 4 the PL functions of the Bino mass parameter  $M_1$  correlated with the Singlino mass  $m_N$ , the total Higgsino mass parameter  $\mu_{tot}$ , and the Wino mass  $M_2$ . From the left panel of Fig. 4, one observes that the  $1\sigma$  region of  $M_1$  in **Scenario I** lies in the range  $-500 \text{ GeV} \lesssim M_1 \lesssim -300 \text{ GeV}$ . In this scenario, the relic density is obtained either through efficient  $s$ -channel resonance annihilation  $\tilde{\chi}_1^0 \tilde{\chi}_1^0 \rightarrow h_s A_H$ , which is enhanced when  $2m_{\tilde{\chi}_1^0} \simeq m_{A_s} \simeq 800 \text{ GeV}$ , or through coannihilation with Singlino-dominated  $\tilde{\chi}_2^0$  states. In the latter case, the dominant processes are  $\tilde{\chi}_2^0 \tilde{\chi}_2^0, \tilde{\chi}_1^0 \tilde{\chi}_2^0 \rightarrow h_s A_H$ , which together yield the correct DM abundance. In contrast, in **Scenario II**, the  $2\sigma$  region favors heavier and more negative  $M_1$  values  $M_1 \lesssim -500 \text{ GeV}$ . As seen from the middle panel of Fig. 4, the relic density is predominantly controlled by coannihilation with Higgsino-dominated  $\tilde{\chi}_2^0$  or  $\tilde{\chi}_1^\pm$  states. The leading channels in this case are  $\tilde{\chi}_1^+ \tilde{\chi}_1^-, \tilde{\chi}_2^0 \tilde{\chi}_2^0 \rightarrow h_s A_s$ , as well as processes such as  $\tilde{\chi}_1^+ \tilde{\chi}_2^0 \rightarrow u\bar{d}, h_s W^+$ . These channels efficiently reduce the relic abundance to the observed level.

In Fig. 5, the SI and SD DM–nucleon scattering cross sections are shown as functions of the LSP mass  $m_{\tilde{\chi}_1^0}$  in the left and right panels, respectively. For comparison, we overlay the latest 90% CL upper limits from the combined WS2024+WS2022 analysis of the LZ experiment [156, 157], the projected sensitivities for future LZ runs [180], and the expected

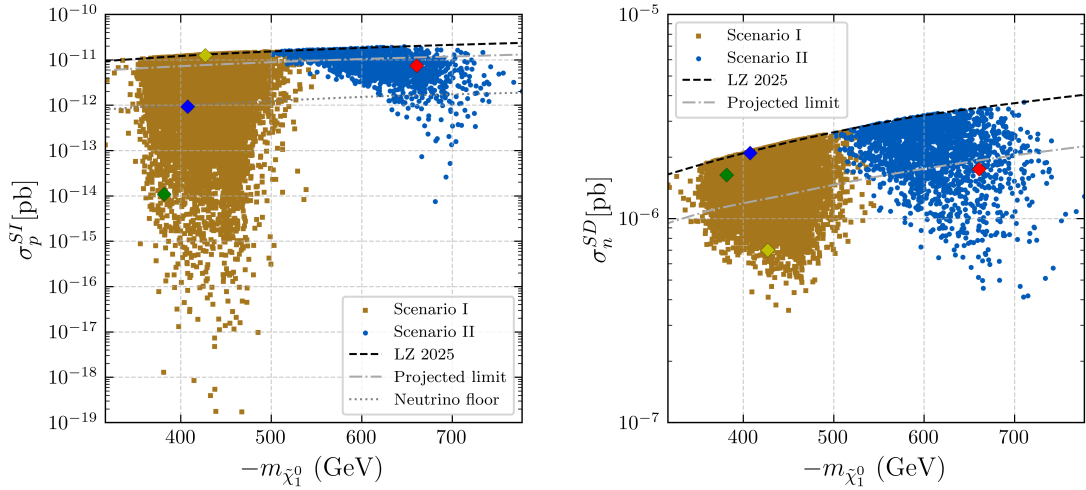


**Figure 5.** Spin-independent (SI) and spin-dependent (SD) DM–nucleon scattering cross sections,  $\sigma_p^{\text{SI}}$  (left) and  $\sigma_n^{\text{SD}}$  (right), as functions of the LSP mass  $m_{\tilde{\chi}_1^0}$ . Dashed black lines show the 90% C.L. upper limits from the 2025 LZ results [156, 157], dashed-dotted grey lines indicate the projected LZ sensitivities for future runs [180], and dotted lines denote the neutrino floor [181]. Amber squares and blue dots correspond to **Scenario I** and **Scenario II**, respectively. Colored diamonds represent the four benchmark points shown in Figs. 1–4.

neutrino background [181]. The left panel illustrates that most viable samples lie well below both the current and projected SI limits. Within **Scenario I**, samples with  $\sigma(gg \rightarrow H \rightarrow hh_s \rightarrow \gamma\gamma b\bar{b}) > 0.09$  fb in the lower  $m_{\tilde{\chi}_1^0}$  region generally predict smaller  $\sigma_p^{\text{SI}}$  compared with **Scenario II**, whose points satisfying  $\chi_{\sigma_{\gamma\gamma b\bar{b}}}^2 + \chi_{\mu_{\gamma\gamma}}^2 \leq 6.18$  appear at larger  $m_{\tilde{\chi}_1^0}$ . The right panel shows that while all samples remain consistent with current SD bounds, the projected sensitivity can probe roughly half of them.

To further clarify the model’s interpretation of the observed excesses, four benchmark points—P1, P2, and P3 from **Scenario I**, and P4 from **Scenario II**—are selected to illustrate representative behaviors. These benchmark points are highlighted as blue, yellow, green, and red diamonds, respectively, in all relevant figures, and their detailed properties are listed in Tables. 2 and 3. The phenomenological characteristics of these benchmarks are summarized as follows:

- P1 simultaneously accommodates the  $\sigma_{\gamma\gamma b\bar{b}}$  excess near 650 GeV, as well as the excesses in  $\mu_{\gamma\gamma}$  and  $\mu_{b\bar{b}}$  near 95 GeV, all at the  $2\sigma$  level (treated individually rather than in combination).
- P2 provides a  $2\sigma$  interpretation of the combined excesses in  $\sigma_{\gamma\gamma b\bar{b}}$  and  $\mu_{b\bar{b}}$ , and predicts  $\mu_{\gamma\gamma}$  within  $2.4\sigma$ .
- P3 successfully explains the  $\mu_{\gamma\gamma}$  and  $\mu_{b\bar{b}}$  excesses at the  $2\sigma$  level, while slightly exceeding the  $2\sigma$  preferred region of  $\sigma_{\gamma\gamma b\bar{b}}$ .

- P4 yields a  $2\sigma$  interpretation of the combined  $\sigma_{\gamma\gamma b\bar{b}}$  and  $\mu_{\gamma\gamma}$  anomalies, with  $\mu_{b\bar{b}}$  falling within the  $2\sigma$  interval as well.

Concerning DM physics, the  $\tilde{\chi}_1^0$  candidate in P1, P2 and P3 achieves the observed relic abundance primarily via the  $A_s$ -funnel mechanism, annihilating into the  $h_s A_H$  final state. In particular, P1 and P3 rely on coannihilation processes involving a  $\tilde{S}$ -like  $\tilde{\chi}_2^0$ , whereas P4 requires coannihilation with  $\tilde{H}$ -like electroweakinos. In terms of direct detection prospects, P1 and P3 may be probed by future SD searches. However, their SI scattering cross sections are strongly suppressed and lie below the neutrino floor, due to significant cancellations among different contributions to the  $\tilde{\chi}_1^0$ -Higgs boson coupling. In contrast, P2 predicts an extremely small SD neutron scattering cross section, as low as  $6.9 \times 10^{-7}$  pb, resulting from a highly suppressed  $\tilde{\chi}_1^0$ -Z gauge boson coupling characterized by  $N_{13}^2 - N_{14}^2 \simeq 0.004$ .

Regarding constraints from the LHC searches for SUSY, simulation results of electroweakino productions, utilizing the package `CheckMATE-2.0.26`, consistently indicate that the constraints from LHC searches for new physics are minimal. The calculated  $R$ -values for all benchmark points are less than 0.35, confirming that the parameter space is safely compliant with existing 95% CL limits. The basic reason for these weak restrictions is that the interpretation of the scalar excesses primarily relies on Higgs sector mixing effects rather than sizable contributions from loop effects involving light SUSY particles. Specific analysis of the benchmark points highlights the dominant search channels:

- P1, P2 and P3: The most significant signal region is G05 from the CMS report CMS-SUS-16-039 [182]. This targets events with at least four leptons, no  $\tau$  leptons, and high missing transverse momentum ( $p_T^{\text{miss}} \geq 200$  GeV).
- P4: This point yields the lowest  $R$  value because it predicts a highly compressed mass spectrum, with a mass difference  $\Delta m(\tilde{\chi}_2^0, \tilde{\chi}_1^0) \lesssim 20$  GeV, making the decay products too soft to be effectively detected by current searches.

For each benchmark, the most significant signal regions, corresponding  $R$  values, and the associated experimental analyses are precisely listed in the bottom rows of Table. 2 and Table. 3.

In addition, we further investigate the constraints from electroweak precision observables on the interpretation of the observed anomalies. For each viable parameter point, the oblique parameters  $S$ ,  $T$  and  $U$  are evaluated using the `SPheno` package and confronted with the results of the global electroweak fit [159]:

$$S = 0.021 \pm 0.096, \quad T = 0.040 \pm 0.120, \quad U = 0.008 \pm 0.092. \quad (3.3)$$

with a strong positive correlation between  $S$  and  $T$ ,  $\rho_{ST} = 0.91$ , and negative correlations between  $S$  and  $U$ ,  $\rho_{SU} = -0.62$ , as well as between  $T$  and  $U$ ,  $\rho_{TU} = -0.83$ . We calculate the  $\chi^2$  value assuming three degrees of freedom and require agreement with the fit result within a confidence level of  $2\sigma$ . Under this criterion, the allowed ranges of the oblique parameters relevant for the interpretation of the anomalies are found to be  $0.013 \lesssim S \lesssim 0.049$ ,  $-0.017 \lesssim T \lesssim 0.0002$ ,  $U \simeq 0.0$ . We find that electroweak precision tests exclude only

**Table 2.** Details of the benchmark points P1 and P2 from **Scenario I**, represented as blue and yellow diamonds, respectively, in all figures. P1 simultaneously accommodates the  $\sigma_{\gamma\gamma b\bar{b}}$  excess near 650 GeV, as well as the excesses in  $\mu_{\gamma\gamma}$  and  $\mu_{b\bar{b}}$  near 95 GeV at the  $2\sigma$  level, while satisfying all applied constraints. P2 provides a  $2\sigma$  combined interpretation of the  $\sigma_{\gamma\gamma b\bar{b}}$  and  $\mu_{b\bar{b}}$  excesses.

Benchmark Point P1				Benchmark Point P2			
$\mu_{tot}$	592.4 GeV	$\lambda$	0.579	$\mu_{tot}$	672.9 GeV	$\lambda$	0.599
$\mu$	228.7 GeV	$\kappa$	0.150	$\mu$	365.6 GeV	$\kappa$	0.214
$\mu'$	-709.1 GeV	$\delta$	0.016	$\mu'$	-755.8 GeV	$\delta$	0.016
$M_1$	-404.3 GeV	$\tan\beta$	1.557	$M_1$	-423.3 GeV	$\tan\beta$	1.493
$M_2$	628.3 GeV	$A_\lambda$	1803 GeV	$M_2$	842.0 GeV	$A_\lambda$	1969 GeV
$m_A$	603.7 GeV	$A_\kappa$	1808 GeV	$m_A$	626.4 GeV	$A_\kappa$	1893 GeV
$m_B$	113.4 GeV	$A_t$	2005 GeV	$m_B$	118.5 GeV	$A_t$	1662 GeV
$m_N$	-521.1 GeV			$m_N$	-536.2 GeV		
$m_{\chi_1^0}$	-407.0 GeV	$m_{h_s}$	95.0 GeV	$m_{\chi_1^0}$	-427.2 GeV	$m_{h_s}$	95.71 GeV
$m_{\chi_2^0}$	-451.6 GeV	$m_h$	127.1 GeV	$m_{\chi_2^0}$	-478.4 GeV	$m_h$	124.1 GeV
$m_{\chi_3^0}$	547.0 GeV	$m_H$	655.6 GeV	$m_{\chi_3^0}$	654.2 GeV	$m_H$	664.9 GeV
$m_{\chi_4^0}$	-660.0 GeV	$m_{A_H}$	512.1 GeV	$m_{\chi_4^0}$	-728.4 GeV	$m_{A_H}$	495.5 GeV
$m_{\chi_5^0}$	707.2 GeV	$m_{A_s}$	878.2 GeV	$m_{\chi_5^0}$	896.6 GeV	$m_{A_s}$	888.6 GeV
$m_{\chi_1^\pm}$	505.7 GeV	$m_{H^\pm}$	635.0 GeV	$m_{\chi_1^\pm}$	652.6 GeV	$m_{H^\pm}$	647.6 GeV
$m_{\chi_2^\pm}$	706.8 GeV			$m_{\chi_2^\pm}$	896.7 GeV		
$\Omega h^2$		0.132		$\Omega h^2$		0.120	
$\sigma_p^{SI}, \sigma_n^{SD}$		$9.2 \times 10^{-49} \text{ cm}^2, 2.0 \times 10^{-42} \text{ cm}^2$		$\sigma_p^{SI}, \sigma_n^{SD}$		$1.2 \times 10^{-47} \text{ cm}^2, 6.9 \times 10^{-43} \text{ cm}^2$	
$\mu_{\gamma\gamma}$		0.081		$\mu_{\gamma\gamma}$		0.048	
$\mu_{b\bar{b}}$		0.230		$\mu_{b\bar{b}}$		0.171	
$\sigma_{\gamma\gamma b\bar{b}}$		0.092 fb		$\sigma_{\gamma\gamma b\bar{b}}$		0.099 fb	
$\sigma(gg \rightarrow H \rightarrow hh_s \rightarrow \tau\tau b\bar{b})$		1.918 fb		$\sigma(gg \rightarrow H \rightarrow hh_s \rightarrow \tau\tau b\bar{b})$		2.356 fb	
$\sigma(gg \rightarrow H \rightarrow h_s h_s \rightarrow b\bar{b}b\bar{b})$		0.023 fb		$\sigma(gg \rightarrow H \rightarrow h_s h_s \rightarrow b\bar{b}b\bar{b})$		1.078 fb	
$\sigma(gg \rightarrow A_H \rightarrow Zh \rightarrow Zb\bar{b})$		7.362 fb		$\sigma(gg \rightarrow A_H \rightarrow Zh \rightarrow Zb\bar{b})$		6.336 fb	
$\sigma(gg \rightarrow A_H \rightarrow Zh_s \rightarrow tb\bar{b})$		7.454 fb		$\sigma(gg \rightarrow A_H \rightarrow Zh_s \rightarrow tb\bar{b})$		8.549 fb	
$C_{h_s gg}, C_{h_s VV}, C_{h_s \gamma\gamma}, C_{h_s t\bar{t}}, C_{h_s b\bar{b}}$		0.388, 0.461, 0.386, 0.382, 0.643		$C_{h_s gg}, C_{h_s VV}, C_{h_s \gamma\gamma}, C_{h_s t\bar{t}}, C_{h_s b\bar{b}}$		0.314, 0.395, 0.375, 0.314, 0.577	
$C_{h_{gg}}, C_{h_{VV}}, C_{h_{\gamma\gamma}}, C_{h_{t\bar{t}}}, C_{h_{b\bar{b}}}$		0.973, 0.887, 0.909, 0.919, 0.810		$C_{h_{gg}}, C_{h_{VV}}, C_{h_{\gamma\gamma}}, C_{h_{t\bar{t}}}, C_{h_{b\bar{b}}}$		0.955, 0.918, 0.936, 0.947, 0.855	
$C_{H_{gg}}, C_{H_{VV}}, C_{H_{\gamma\gamma}}, C_{H_{t\bar{t}}}, C_{H_{b\bar{b}}}$		0.559, 0.009, 4.001, 0.647, 1.534		$C_{H_{gg}}, C_{H_{VV}}, C_{H_{\gamma\gamma}}, C_{H_{t\bar{t}}}, C_{H_{b\bar{b}}}$		0.582, 0.009, 3.843, 0.673, 1.472	
$C_{A_H gg}, C_{A_H \gamma\gamma}, C_{A_H t\bar{t}}, C_{A_H b\bar{b}}$		0.650, 1.289, 0.538, 1.305		$C_{A_H gg}, C_{A_H \gamma\gamma}, C_{A_H t\bar{t}}, C_{A_H b\bar{b}}$		0.673, 1.152, 0.545, 1.215	
$N_{11}, N_{12}, N_{13}, N_{14}, N_{15}$		-0.988, -0.001, 0.102, 0.045, -0.107		$N_{11}, N_{12}, N_{13}, N_{14}, N_{15}$		0.994, -0.001, 0.073, 0.020, -0.077	
$N_{21}, N_{22}, N_{23}, N_{24}, N_{25}$		-0.146, 0.009, 0.365, 0.397, -0.829		$N_{21}, N_{22}, N_{23}, N_{24}, N_{25}$		-0.097, 0.006, 0.300, 0.327, -0.891	
$N_{31}, N_{32}, N_{33}, N_{34}, N_{35}$		-0.036, -0.583, 0.580, -0.567, -0.017		$N_{31}, N_{32}, N_{33}, N_{34}, N_{35}$		-0.038, -0.337, 0.668, -0.662, -0.016	
$N_{41}, N_{42}, N_{43}, N_{44}, N_{45}$		0.029, -0.010, -0.596, -0.586, -0.548		$N_{41}, N_{42}, N_{43}, N_{44}, N_{45}$		0.024, -0.008, -0.636, -0.629, -0.447	
$N_{51}, N_{52}, N_{53}, N_{54}, N_{55}$		0.026, -0.812, -0.405, 0.419, 0.009		$N_{51}, N_{52}, N_{53}, N_{54}, N_{55}$		0.011, -0.941, -0.231, 0.245, 0.004	
Annihilations		Fractions [%]		Annihilations		Fractions [%]	
$\tilde{\chi}_1^0 \tilde{\chi}_2^0 \rightarrow H^\pm W^\mp / h_s A_H / t\bar{t} / HZ$		20.8/13.5/7.5/7.2		$\tilde{\chi}_1^0 \tilde{\chi}_1^0 \rightarrow h_s A_H / H^\pm W^\mp / t\bar{t} / HZ / h_s Z$		31.7/26.1/14.7/9.4/2.0	
$\tilde{\chi}_1^0 \tilde{\chi}_1^0 \rightarrow h_s A_H / H^\pm W^\mp / t\bar{t} / HZ$		11.3/10.3/9.8/7.2		$\tilde{\chi}_1^0 \tilde{\chi}_2^0 \rightarrow H^\pm W^\mp / h_s A_H / HZ / t\bar{t}$		4.2/3.1/1.5/1.0	
$\tilde{\chi}_2^0 \tilde{\chi}_2^0 \rightarrow h_s A_H / t\bar{t}$		2.7/2.5					
Decays		Branching ratios [%]		Decays		Branching ratios [%]	
$h_s \rightarrow b\bar{b} / \tau^+ \tau^- / c\bar{c} / gg / W^+ W^- / \gamma\gamma$		87.2/9.65/1.48/1.39/0.10/0.08		$h_s \rightarrow b\bar{b} / \tau^+ \tau^- / c\bar{c} / gg / W^+ W^- / \gamma\gamma$		87.6/9.71/1.23/1.16/0.12/0.07	
$h \rightarrow b\bar{b} / W^+ W^- / \tau^+ \tau^- / gg / ZZ / c\bar{c} / \gamma\gamma$		52.1/29.4/6.06/5.53/3.35/3.17/0.029		$h \rightarrow b\bar{b} / W^+ W^- / \tau^+ \tau^- / gg / ZZ / c\bar{c} / \gamma\gamma$		58.3/23.2/6.76/5.62/2.44/3.37/0.028	
$H \rightarrow t\bar{t} / A_H Z / h h_s / h h$		72.3/13.3/9.02/4.99		$H \rightarrow t\bar{t} / A_H Z / h h_s / h h$		65.4/20.6/9.80/3.50	
$A_H \rightarrow t\bar{t} / h_s Z / h Z$		93.7/5.07/0.84		$A_H \rightarrow t\bar{t} / h_s Z / h Z$		94.4/4.70/0.52	
$A_s \rightarrow H^\pm W^\mp / h_s A_H / t\bar{t} / HZ$		40.4/25.3/16.4/14.3		$A_s \rightarrow H^\pm W^\mp / h_s A_H / t\bar{t} / HZ$		35.6/ 31.6/16.2/13.2	
$H^\pm \rightarrow t\bar{b} / A_H W^\pm / h_s W^\pm / h W^\pm$		81.8/8.6/8.1/1.4		$H^\pm \rightarrow t\bar{b} / A_s W^\pm / h_s W^\pm / h W^\pm$		74.8/16.7/7.63/0.89	
$\tilde{\chi}_2^0 \rightarrow \tilde{\chi}_1^0 Z^*$		100		$\tilde{\chi}_2^0 \rightarrow \tilde{\chi}_1^0 Z^*$		100	
$\tilde{\chi}_3^0 \rightarrow \tilde{\chi}_1^0 Z / \tilde{\chi}_2^0 Z / \tilde{\chi}_1^0 h_s / \tilde{\chi}_1^0 h$		61.0/35.7/1.9/1.3		$\tilde{\chi}_3^0 \rightarrow \tilde{\chi}_2^0 Z / \tilde{\chi}_1^0 Z / \tilde{\chi}_1^0 h / \tilde{\chi}_1^0 h_s$		93.7/4.71/1.14/0.22	
$\tilde{\chi}_4^0 \rightarrow \tilde{\chi}_1^+ W^\mp / \tilde{\chi}_2^0 h / \tilde{\chi}_3^0 h_s / \tilde{\chi}_3^0 Z / \tilde{\chi}_1^0 h$		32.8/36.3/17.0/9.07/2.7		$\tilde{\chi}_4^0 \rightarrow \tilde{\chi}_2^0 h / \tilde{\chi}_2^0 h_s / \tilde{\chi}_1^0 h / \tilde{\chi}_1^0 Z$		76.2/17.9/2.86/1.57	
$\tilde{\chi}_5^0 \rightarrow \tilde{\chi}_2^\pm W^\mp / \tilde{\chi}_2^0 Z / \tilde{\chi}_3^0 h_s / \tilde{\chi}_2^0 Z$		41.2/40.7/14.8/2.3		$\tilde{\chi}_5^0 \rightarrow \tilde{\chi}_2^\pm W^\mp / \tilde{\chi}_2^0 Z / \tilde{\chi}_3^0 h_s / \tilde{\chi}_4^0 Z$		47.5/22.6/14.8/6.30	
$\tilde{\chi}_1^\pm \rightarrow \tilde{\chi}_1^0 W^\pm$		100		$\tilde{\chi}_1^\pm \rightarrow \tilde{\chi}_1^0 W^\pm$		100	
$\tilde{\chi}_2^\pm \rightarrow \tilde{\chi}_2^0 W^\pm / \tilde{\chi}_3^0 W^\pm / \tilde{\chi}_1^\pm Z / \tilde{\chi}_1^\pm h_s$		39.6/23.6/19.6/14.7		$\tilde{\chi}_2^\pm \rightarrow \tilde{\chi}_3^0 W^\pm / \tilde{\chi}_1^\pm Z / \tilde{\chi}_2^0 W^\pm / \tilde{\chi}_1^\pm h_s$		25.7/23.6/21.2/14.2	
$S, T, U$		0.046, -0.014, -0.000		$S, T, U$		0.040, -0.013, -0.001	
$R$ value		0.24		$R$ value		0.23	
Signal Region		G05 in CMS-SUS-16-039 [183]		Signal Region		G05 in CMS-SUS-16-039 [183]	

a small fraction of the parameter space in **Scenario I**, without significantly altering the overall phenomenological picture. In this scenario, the mass splitting between the charged Higgs bosons and the neutral CP-odd Higgs boson,  $\Delta m(H^\pm, A_H)$ , can reach values as large as about 170 GeV. This feature can be understood by noting that **Scenario I** allows for relatively large mixing induced by the enhancement of  $A_\lambda - m_N$  (see the discussion of the lower-left panel of Fig. 3). We present three representative benchmark points, P1, P2, and P3 in Table. 2, which satisfy all electroweak precision constraints in **Scenario I**. In

**Table 3.** Details of the benchmark points P3 from **Scenario I** and P4 from **Scenario II** that are denoted as diamonds colored green and red, respectively, in all presented figures. P3 successfully explains the  $\mu_{\gamma\gamma}$  and  $\mu_{b\bar{b}}$  excesses at the  $2\sigma$  level, while slightly exceeding the  $2\sigma$  preferred region of  $\sigma_{\gamma\gamma b\bar{b}}$ . P4 yields a  $2\sigma$  interpretation of the combined  $\sigma_{\gamma\gamma b\bar{b}}$  and  $\mu_{\gamma\gamma}$  anomalies, with  $\mu_{b\bar{b}}$  falling within the  $2\sigma$  interval as well. In the listed annihilation final states,  $d_i$  and  $u_i$  denote the  $i$ th generation of down-type and up-type quarks, respectively.

Benchmark Point P3				Benchmark Point P4			
$\mu_{tot}$	600.8 GeV	$\lambda$	0.622	$\mu_{tot}$	711.8 GeV	$\lambda$	0.688
$\mu$	277.1 GeV	$\kappa$	0.213	$\mu$	581.5 GeV	$\kappa$	-0.094
$\mu'$	-703.3 GeV	$\delta$	-0.001	$\mu'$	750.4 GeV	$\delta$	0.033
$M_1$	-378.0 GeV	$\tan\beta$	1.442	$M_1$	-656.4 GeV	$\tan\beta$	1.467
$M_2$	532.8 GeV	$A_\lambda$	1765 GeV	$M_2$	855.4 GeV	$A_\lambda$	763.8 GeV
$m_A$	641.1 GeV	$A_\kappa$	1702 GeV	$m_A$	616.0 GeV	$A_\kappa$	-1955 GeV
$m_B$	110.0 GeV	$A_t$	1441 GeV	$m_B$	97.57 GeV	$A_t$	1082 GeV
$m_N$	-481.0 GeV			$m_N$	714.9 GeV		
$m_{\tilde{\chi}_1^0}$	-381.7 GeV	$m_{h_s}$	94.86 GeV	$m_{\tilde{\chi}_1^0}$	-660.9 GeV	$m_{h_s}$	95.37 GeV
$m_{\tilde{\chi}_2^0}$	-416.1 GeV	$m_h$	126.4 GeV	$m_{\tilde{\chi}_2^0}$	679.0 GeV	$m_h$	127.3 GeV
$m_{\tilde{\chi}_3^0}$	502.3 GeV	$m_H$	661.1 GeV	$m_{\tilde{\chi}_3^0}$	-728.8 GeV	$m_H$	629.0 GeV
$m_{\tilde{\chi}_4^0}$	661.4 GeV	$m_{A_H}$	514.1 GeV	$m_{\tilde{\chi}_4^0}$	730.3 GeV	$m_{A_H}$	615.6 GeV
$m_{\tilde{\chi}_5^0}$	-662 GeV	$m_{A_s}$	876.3 GeV	$m_{\tilde{\chi}_5^0}$	913.3 GeV	$m_{A_s}$	809.9 GeV
$m_{\tilde{\chi}_1^\pm}$	501.7 GeV	$m_{H^\pm}$	650.0 GeV	$m_{\tilde{\chi}_1^\pm}$	688.9 GeV	$m_{H^\pm}$	617.9 GeV
$m_{\tilde{\chi}_2^\pm}$	661.2 GeV			$m_{\tilde{\chi}_2^\pm}$	913.1 GeV		
$\Omega h^2$		0.104		$\Omega h^2$		0.114	
$\sigma_p^{SI}, \sigma_n^{SD}$		$1.1 \times 10^{-50} \text{ cm}^2, 1.6 \times 10^{-42} \text{ cm}^2$		$\sigma_p^{SI}, \sigma_n^{SD}$		$7.4 \times 10^{-48} \text{ cm}^2, 1.7 \times 10^{-42} \text{ cm}^2$	
$\mu_{\gamma\gamma}$		0.088		$\mu_{\gamma\gamma}$		0.195	
$\mu_{b\bar{b}}$		0.225		$\mu_{b\bar{b}}$		0.014	
$\sigma_{\gamma\gamma b\bar{b}}$		0.074 fb		$\sigma_{\gamma\gamma b\bar{b}}$		0.045 fb	
$\sigma(gg \rightarrow H \rightarrow hh_s \rightarrow \tau\bar{\tau}b\bar{b})$		1.632 fb		$\sigma(gg \rightarrow H \rightarrow hh_s \rightarrow \tau\bar{\tau}b\bar{b})$		1.262 fb	
$\sigma(gg \rightarrow H \rightarrow h_s h_s \rightarrow b\bar{b}b\bar{b})$		0.071 fb		$\sigma(gg \rightarrow H \rightarrow h_s h_s \rightarrow b\bar{b}b\bar{b})$		36.75 fb	
$\sigma(gg \rightarrow A_H \rightarrow Zh \rightarrow Zb\bar{b})$		5.086 fb		$\sigma(gg \rightarrow A_H \rightarrow Zh \rightarrow Zb\bar{b})$		0.579 fb	
$\sigma(gg \rightarrow A_H \rightarrow Zh_s \rightarrow llb\bar{b})$		5.414 fb		$\sigma(gg \rightarrow A_H \rightarrow Zh_s \rightarrow llb\bar{b})$		0.966 fb	
$C_{h_s gg}, C_{h_s VV}, C_{h_s \gamma\gamma}, C_{h_s tt}, C_{h_s b\bar{b}}$		0.391, 0.456, 0.431, 0.386, 0.603		$C_{h_s gg}, C_{h_s VV}, C_{h_s \gamma\gamma}, C_{h_s tt}, C_{h_s b\bar{b}}$		0.280, 0.145, 0.172, 0.254, 0.089	
$C_{h_s gg}, C_{h_s VV}, C_{h_s \gamma\gamma}, C_{h_s tt}, C_{h_s b\bar{b}}$		0.924, 0.889, 0.914, 0.918, 0.830		$C_{h_s gg}, C_{h_s VV}, C_{h_s \gamma\gamma}, C_{h_s tt}, C_{h_s b\bar{b}}$		0.967, 0.989, 1.006, 0.966, 1.039	
$C_{H gg}, C_{H VV}, C_{H \gamma\gamma}, C_{H tt}, C_{H b\bar{b}}$		0.604, 0.010, 4.129, 0.699, 1.423		$C_{H gg}, C_{H VV}, C_{H \gamma\gamma}, C_{H tt}, C_{H b\bar{b}}$		0.593, 0.011, 4.530, 0.683, 1.437	
$C_{A_H gg}, C_{A_H VV}, C_{A_H \gamma\gamma}, C_{A_H tt}, C_{A_H b\bar{b}}$		0.683, 1.380, 0.568, 1.181		$C_{A_H gg}, C_{A_H VV}, C_{A_H \gamma\gamma}, C_{A_H tt}, C_{A_H b\bar{b}}$		0.745, 4.688, 0.681, 1.467	
$N_{11}, N_{12}, N_{13}, N_{14}, N_{15}$		0.988, -0.002, 0.034, 0.032, -0.116		$N_{11}, N_{12}, N_{13}, N_{14}, N_{15}$		-0.992, 0.000, -0.108, -0.064, -0.001	
$N_{21}, N_{22}, N_{23}, N_{24}, N_{25}$		-0.144, 0.008, 0.318, 0.351, -0.869		$N_{21}, N_{22}, N_{23}, N_{24}, N_{25}$		-0.113, -0.027, -0.317, -0.613, 0.452	
$N_{31}, N_{32}, N_{33}, N_{34}, N_{35}$		-0.028, -0.815, 0.416, -0.401, -0.012		$N_{31}, N_{32}, N_{33}, N_{34}, N_{35}$		-0.122, 0.010, 0.698, 0.702, 0.008	
$N_{41}, N_{42}, N_{43}, N_{44}, N_{45}$		0.034, -0.578, -0.572, 0.580, 0.013		$N_{41}, N_{42}, N_{43}, N_{44}, N_{45}$		-0.012, -0.200, 0.340, -0.237, -0.888	
$N_{51}, N_{52}, N_{53}, N_{54}, N_{55}$		0.023, -0.010, -0.623, -0.615, -0.481		$N_{51}, N_{52}, N_{53}, N_{54}, N_{55}$		0.010, -0.927, -0.260, 0.268, 0.038	
Annihilations		Fractions [%]		Annihilations		Fractions [%]	
$\tilde{\chi}_2^0 \tilde{\chi}_2^0 \rightarrow h_s A_H / H^\pm W^\mp / t\bar{t} / HZ$		26.3/25.4/12.1/9.7		$\tilde{\chi}_2^0 \tilde{\chi}_2^0 \rightarrow d_i \bar{u}_i / h_s W^- / hW^- / A_s W^- / A_H W^-$		11/4.4/2.9/2.9/1.6	
$\tilde{\chi}_1^0 \tilde{\chi}_2^0 \rightarrow h_s A_H / H^\pm W^\mp / t\bar{t} / HZ$		5.2/4.3/3.8/1.4		$\tilde{\chi}_2^0 \tilde{\chi}_2^0 \rightarrow h_s A_s / HZ / t\bar{t} / W^+ W^-$		5.7/1.7/1.6/1.5	
$\tilde{\chi}_1^0 \tilde{\chi}_1^0 \rightarrow t\bar{t} / h_s A_H$		2.9/2.7		$\tilde{\chi}_1^+ \tilde{\chi}_1^+ \rightarrow h_s A_s / W^+ W^- / t\bar{t}$		4.8/1.4/1.3	
Decays		Branching ratios [%]		Decays		Branching ratios [%]	
$h_s \rightarrow b\bar{b} / \tau^+ \tau^- / c\bar{c} / gg / W^+ W^- / \gamma\gamma$		86.8/9.61/1.68/1.59/0.11/0.08		$h_s \rightarrow b\bar{b} / gg / c\bar{c} / \tau^+ \tau^- / W^+ W^- / \gamma\gamma$		51.4/22.5/19.7/5.69/0.37/0.36	
$h \rightarrow b\bar{b} / W^+ W^- / \tau^+ \tau^- / gg / c\bar{c} / ZZ / \gamma\gamma$		54.3/27.4/6.31/5.41/3.13/3.08/0.28		$h \rightarrow b\bar{b} / W^+ W^- / \tau^+ \tau^- / gg / ZZ / c\bar{c} / \gamma\gamma$		57.9/25.7/6.74/4.10/2.91/2.36/0.31	
$H \rightarrow t\bar{t} / A_H Z / h h_s / h h$		76.5/12.8/6.6/3.8		$H \rightarrow t\bar{t} / h_s h_s / h h_s / h h$		67.8/25.1/6.6/0.20	
$A_H \rightarrow t\bar{t} / h_s Z / h Z$		95.8/3.4/0.5		$A_H \rightarrow t\bar{t} / h_s Z / h Z$		87.5/11.7/0.5	
$A_s \rightarrow H^\pm W^\mp / h_s A_H / t\bar{t} / h_s Z$		33.2/29.6/19.4/2.2		$A_s \rightarrow h_s A_H / H^\pm W^\mp / t\bar{t} / h A_H$		39.6/20.9/18.7/8.6	
$H^\pm \rightarrow t\bar{b} / A_H W^\pm / h_s W^\pm / h W^\pm$		82.5/11.0/5.6/0.9		$H^\pm \rightarrow t\bar{b} / h_s W^\pm / h W^\pm$		85.9/13.5/0.59	
$\tilde{\chi}_2^0 \rightarrow \tilde{\chi}_1^0 Z^*$		100		$\tilde{\chi}_2^0 \rightarrow \tilde{\chi}_1^0 Z^*$		100	
$\tilde{\chi}_3^0 \rightarrow \tilde{\chi}_1^0 Z / \tilde{\chi}_1^0 h_s$		74.1/3.5		$\tilde{\chi}_3^0 \rightarrow \tilde{\chi}_2^0 Z / \tilde{\chi}_1^0 W^\mp / \tilde{\chi}_1^0 Z$		49.8/48.6/3.13	
$\tilde{\chi}_4^0 \rightarrow \tilde{\chi}_2^0 Z / \tilde{\chi}_1^0 W^\mp / \tilde{\chi}_3^0 h / \tilde{\chi}_3^0 h_s$		48.6/36.9/6.4/5.1		$\tilde{\chi}_4^0 \rightarrow \tilde{\chi}_1^0 W^\mp / \tilde{\chi}_3^0 h_s / \tilde{\chi}_3^0 Z$		69.7/15.6/5.80	
$\tilde{\chi}_5^0 \rightarrow \tilde{\chi}_1^0 W^\mp / \tilde{\chi}_3^0 h / \tilde{\chi}_3^0 Z / \tilde{\chi}_3^0 h_s$		39.5/32.9/16.5/8.2		$\tilde{\chi}_5^0 \rightarrow \tilde{\chi}_2^0 W^\mp / \tilde{\chi}_3^0 Z / \tilde{\chi}_3^0 h / \tilde{\chi}_1^0 h_s$		55.7/16.7/15.9/6.61	
$\tilde{\chi}_1^\pm \rightarrow \tilde{\chi}_1^0 W^{*\pm} / \tilde{\chi}_2^0 W^{*\pm}$		60.6/39.4		$\tilde{\chi}_1^\pm \rightarrow \tilde{\chi}_1^0 W^{*\pm} / \tilde{\chi}_2^0 W^{*\pm}$		75.2/24.7	
$\tilde{\chi}_2^\pm \rightarrow \tilde{\chi}_1^0 W^\pm / \tilde{\chi}_3^0 W^\pm / \tilde{\chi}_1^\pm Z / \tilde{\chi}_1^\pm h / \tilde{\chi}_1^\pm h_s$		47.7/20.7/17.1/6.4/5.1		$\tilde{\chi}_2^\pm \rightarrow \tilde{\chi}_1^\pm Z / \tilde{\chi}_2^0 W^\pm / \tilde{\chi}_1^\pm h / \tilde{\chi}_3^0 W^\pm / \tilde{\chi}_4^0 W^\pm$		27.4/22.4/19.4/17.3/6.43	
$S, T, U$		0.033, -0.010, -0.000		$S, T, U$		0.279, -0.051, 0.008	
$R$ value		0.21		$R$ value		0.02	
Signal Region		G05 in CMS-SUS-16-039 [183]		Signal Region		SR2-stop-3high-pt-1 in CMS-SUS-16-048 [182]	

contrast, the oblique parameters impose much more stringent constraints on **Scenario II**, excluding more than half of the sampled parameter points. As an illustrative example of an excluded configuration, we provide the detailed properties of benchmark point P4 in Table. 3, which fails to satisfy the electroweak precision bounds.

## 4 Conclusion

The  $\mu_{\gamma\gamma}$  excess reported by CMS and ATLAS and the  $\mu_{b\bar{b}}$  excess observed at LEP hint in a compatible way at the existence of a light Higgs boson near 95 GeV. In parallel, an excess in the resonant production of SM-like plus BSM Higgs bosons in the diphoton plus  $b\bar{b}$  channel by CMS suggests an extra heavy Higgs bosons near 650 GeV. This research rigorously investigated the capacity of the GNMSSM to simultaneously explain the 95 GeV and 650 GeV excesses while providing a proper DM candidate with correct DM relic abundance. We adopt a framework in which the light singlet-like  $CP$ -even Higgs boson  $h_s$  accounts for the the 95 GeV anomalies, whereas the heavy doublet-like  $CP$ -even Higgs boson  $H$  decays into the SM-like Higgs  $h$  and  $h_s$  to account for the  $\sigma_{\gamma\gamma b\bar{b}}$  excess. This configuration, characterized by small  $\tan\beta$  and large  $\lambda$ , is theoretically well-motivated as it leverages the tree-level singlet-doublet mixing to elevate the mass of the 125 GeV Higgs boson without relying on excessively large radiative corrections. To streamline the parameterization, a small auxiliary factor  $\delta$  is introduced, which substantially improves sampling efficiency without affecting the underlying physics. By performing a comprehensive 12-dimensional parameter scan using state-of-the-art sampling and numerical tools, constrained by a battery of experimental limits including 125 GeV Higgs data,  $B$ -physics, vacuum stability, and the most stringent LZ detection results, we successfully demonstrated the model's viability. The key findings and insights derived from this analysis are summarized below:

1. The best fit in **Scenario I** provides a simultaneous interpretation of the  $\sigma_{\gamma\gamma b\bar{b}}$  excess near 650 GeV and  $\mu_{\gamma\gamma}$  and  $\mu_{b\bar{b}}$  excesses near 95 GeV at the  $2\sigma$  level. Larger values of  $\sigma_{\gamma\gamma b\bar{b}} \gtrsim 0.1$  fb are limited by the CMS search in the  $\tau\bar{\tau}$  plus  $b\bar{b}$  channel.
2. **Scenario II** successfully accommodates the combined  $\sigma_{\gamma\gamma b\bar{b}}$  and  $\mu_{\gamma\gamma}$  excesses at the  $2\sigma$  level, with  $\mu_{\gamma\gamma}$  achieving its central value while  $\mu_{b\bar{b}}$  remains within the  $2\sigma$  interval. However, electroweak precision observables impose significantly stronger constraints on this scenario.
3. The consistent interpretation of the scalar anomalies robustly favors the Bino-dominated  $\tilde{\chi}_1^0$  as the sole DM candidate. The measured relic density is achieved through distinct mechanisms in each scenario: **Scenario I** primarily relies on  $A_s$  funnel annihilation or coannihilation with  $\tilde{S}$ -like  $\tilde{\chi}_2^0$ s, and **Scenario II** favors coannihilation with  $\tilde{H}$ -like  $\tilde{\chi}_2^0$ s or  $\tilde{\chi}_1^\pm$ s.
4. Constraints from LHC searches for electroweakinos have a negligible impact on the viable parameter space. Full Monte Carlo simulations for benchmark points consistently yield low  $R$ -values ( $< 0.30$ ). This is attributed to the relatively heavy electroweakino masses, which reduce production rates, and the compressed mass spectra, which lead to detection-challenging soft final states.
5. The necessary non-zero values for the bilinear parameters  $\mu$  and  $\mu'$  serve as a direct signature that distinguishes the GNMSSM from the minimal  $\mathbb{Z}_3$ -NMSSM and the MSSM.

Beyond these results, we provide prospects for several promising search channels targeting a heavy Higgs boson near 650 GeV, presenting posterior probability density functions for key cross-sections and normalized couplings. These projections offer concrete guidance for testing or excluding the GNMSSM parameter space in future analyses. In addition, the benchmark points identified in this work enable reliable extrapolations to the expected sensitivities of the High-Luminosity LHC. Overall, our results highlight the GNMSSM as a well-motivated extension of the Standard Model that can consistently account for both the observed scalar excesses and a viable DM candidate. This motivates continued experimental efforts in forthcoming collider programs and DM detection experiments.

## Acknowledgements

We thank Prof. Junjie Cao for helpful discussions. This work is supported by the National Natural Science Foundation of China (NNSFC) under Grant No.12447140 and the Natural Science Foundation of Henan Province, China (Grant No. 252300421771, 252300421988)

## A Appendix

**Table A1.** Experimental analyses of the electroweakino production processes considered in this study categorizing by the topologies of the SUSY signals.

Scenario	Final State	Name
$\tilde{\chi}_2^0 \tilde{\chi}_1^\pm \rightarrow WZ \tilde{\chi}_1^0 \tilde{\chi}_1^0$	$n\ell(n \geq 2) + nj(n \geq 0) + E_T^{\text{miss}}$	CMS-SUS-20-001 (137 fb <sup>-1</sup> ) [184]
		ATLAS-2106-01676 (139 fb <sup>-1</sup> ) [185]
		CMS-SUS-17-004 (35.9 fb <sup>-1</sup> ) [186]
		CMS-SUS-16-039 (35.9 fb <sup>-1</sup> ) [182]
		ATLAS-1803-02762 (36.1 fb <sup>-1</sup> ) [187]
		ATLAS-1806-02293 (36.1 fb <sup>-1</sup> ) [188]
$\tilde{\chi}_2^0 \tilde{\chi}_1^\pm \rightarrow Wh \tilde{\chi}_1^0 \tilde{\chi}_1^0$	$n\ell(n \geq 1) + nb(n \geq 0) + nj(n \geq 0) + E_T^{\text{miss}}$	ATLAS-1909-09226 (139 fb <sup>-1</sup> ) [189]
		CMS-SUS-17-004 (35.9 fb <sup>-1</sup> ) [186]
		CMS-SUS-16-039 (35.9 fb <sup>-1</sup> ) [182]
		ATLAS-1812-09432 (36.1 fb <sup>-1</sup> ) [190]
		CMS-SUS-16-034 (35.9 fb <sup>-1</sup> ) [191]
		CMS-SUS-16-045 (35.9 fb <sup>-1</sup> ) [192]
$\tilde{\chi}_1^\mp \tilde{\chi}_1^\pm \rightarrow WW \tilde{\chi}_1^0 \tilde{\chi}_1^0$	$2\ell + E_T^{\text{miss}}$	ATLAS-1908-08215 (139 fb <sup>-1</sup> ) [193]
		CMS-SUS-17-010 (35.9 fb <sup>-1</sup> ) [194]
$\tilde{\chi}_2^0 \tilde{\chi}_1^\pm \rightarrow ZW \tilde{\chi}_1^0 \tilde{\chi}_1^0$ $\tilde{\chi}_1^\pm \tilde{\chi}_1^\mp \rightarrow WW \tilde{\chi}_1^0 \tilde{\chi}_1^0$	$2j(\text{large}) + E_T^{\text{miss}}$	ATLAS-2108-07586 (139 fb <sup>-1</sup> ) [195]
$\tilde{\chi}_2^0 \tilde{\chi}_1^\pm \rightarrow (h/Z)W \tilde{\chi}_1^0 \tilde{\chi}_1^0$ $\tilde{\chi}_2^0 \tilde{\chi}_3^0 \rightarrow (h/Z)Z \tilde{\chi}_1^0 \tilde{\chi}_1^0$	$j(\text{large}) + b(\text{large}) + E_T^{\text{miss}}$	ATLAS-2108-07586 (139 fb <sup>-1</sup> ) [195]
$\tilde{\chi}_2^0 \tilde{\chi}_1^\mp \rightarrow h/ZW \tilde{\chi}_1^0 \tilde{\chi}_1^0, \tilde{\chi}_1^0 \rightarrow \gamma/Z\tilde{G}$ $\tilde{\chi}_1^\pm \tilde{\chi}_1^\mp \rightarrow WW \tilde{\chi}_1^0 \tilde{\chi}_1^0, \tilde{\chi}_1^0 \rightarrow \gamma/Z\tilde{G}$	$2\gamma + n\ell(n \geq 0) + nb(n \geq 0) + nj(n \geq 0) + E_T^{\text{miss}}$	ATLAS-1802-03158 (36.1 fb <sup>-1</sup> ) [196]
$\tilde{\chi}_2^0 \tilde{\chi}_1^\pm \rightarrow ZW \tilde{\chi}_1^0 \tilde{\chi}_1^0, \tilde{\chi}_1^0 \rightarrow h/Z\tilde{G}$ $\tilde{\chi}_1^\pm \tilde{\chi}_1^\mp \rightarrow WW \tilde{\chi}_1^0 \tilde{\chi}_1^0, \tilde{\chi}_1^0 \rightarrow h/Z\tilde{G}$ $\tilde{\chi}_2^0 \tilde{\chi}_1^0 \rightarrow Z \tilde{\chi}_1^0 \tilde{\chi}_1^0, \tilde{\chi}_1^0 \rightarrow h/Z\tilde{G}$ $\tilde{\chi}_1^\mp \tilde{\chi}_1^0 \rightarrow W \tilde{\chi}_1^0 \tilde{\chi}_1^0, \tilde{\chi}_1^0 \rightarrow h/Z\tilde{G}$	$n\ell(n \geq 4) + E_T^{\text{miss}}$	ATLAS-2103-11684 (139 fb <sup>-1</sup> ) [197]
$\tilde{\chi}_i^{0,\pm} \tilde{\chi}_j^{0,\mp} \rightarrow \tilde{\chi}_1^0 \tilde{\chi}_1^0 + \chi_{\text{soft}} \rightarrow ZZ/H\tilde{G}\tilde{G}$	$n\ell(n \geq 2) + nb(n \geq 0) + nj(n \geq 0) + E_T^{\text{miss}}$	CMS-SUS-16-039 (35.9 fb <sup>-1</sup> ) [182]
		CMS-SUS-17-004 (35.9 fb <sup>-1</sup> ) [186]
		CMS-SUS-20-001 (137 fb <sup>-1</sup> ) [184]
$\tilde{\chi}_i^{0,\pm} \tilde{\chi}_j^{0,\mp} \rightarrow \tilde{\chi}_1^0 \tilde{\chi}_1^0 + \chi_{\text{soft}} \rightarrow HH\tilde{G}\tilde{G}$	$n\ell(n \geq 2) + nb(n \geq 0) + nj(n \geq 0) + E_T^{\text{miss}}$	CMS-SUS-16-039 (35.9 fb <sup>-1</sup> ) [182]
		CMS-SUS-17-004 (35.9 fb <sup>-1</sup> ) [186]
$\tilde{\chi}_2^0 \tilde{\chi}_1^\pm \rightarrow W^* Z^* \tilde{\chi}_1^0 \tilde{\chi}_1^0$	$3\ell + E_T^{\text{miss}}$	ATLAS-2106-01676 (139 fb <sup>-1</sup> ) [185]
$\tilde{\chi}_2^0 \tilde{\chi}_1^\pm \rightarrow Z^* W^* \tilde{\chi}_1^0 \tilde{\chi}_1^0$	$2\ell + nj(n \geq 0) + E_T^{\text{miss}}$	ATLAS-1911-12606 (139 fb <sup>-1</sup> ) [183]
		ATLAS-1712-08119 (36.1 fb <sup>-1</sup> ) [198]
		CMS-SUS-16-048 (35.9 fb <sup>-1</sup> ) [199]
$\tilde{\chi}_2^0 \tilde{\chi}_1^\pm + \tilde{\chi}_1^\pm \tilde{\chi}_1^\mp + \tilde{\chi}_1^\pm \tilde{\chi}_1^0$	$2\ell + nj(n \geq 0) + E_T^{\text{miss}}$	ATLAS-1911-12606 (139 fb <sup>-1</sup> ) [183]
		ATLAS-1712-08119 (36.1 fb <sup>-1</sup> ) [198]
		CMS-SUS-16-048 (35.9 fb <sup>-1</sup> ) [199]

## References

- [1] LEP WORKING GROUP FOR HIGGS BOSON SEARCHES, ALEPH, DELPHI, L3, OPAL collaboration, R. Barate et al., *Search for the standard model Higgs boson at LEP*, *Phys. Lett. B* **565** (2003) 61 [[hep-ex/0306033](#)].

- [2] A. Azatov, R. Contino and J. Galloway, *Model-Independent Bounds on a Light Higgs*, *JHEP* **04** (2012) 127 [[1202.3415](#)].
- [3] J. Cao, X. Guo, Y. He, P. Wu and Y. Zhang, *Diphoton signal of the light Higgs boson in natural NMSSM*, *Phys. Rev. D* **95** (2017) 116001 [[1612.08522](#)].
- [4] CMS collaboration, “Search for new resonances in the diphoton final state in the mass range between 80 and 115 GeV in pp collisions at  $\sqrt{s} = 8$  TeV.” [CMS-PAS-HIG-14-037](#), 2015.
- [5] CMS collaboration, “Search for a standard model-like Higgs boson in the mass range between 70 and 110 GeV in the diphoton final state in proton-proton collisions at  $\sqrt{s} = 13$  TeV.” [CMS-PAS-HIG-20-002](#), 2023.
- [6] C. Arcangeletti. on behalf of ATLAS collaboration, LHC Seminar [https://indico.cern.ch/event/1281604/attachments/2660420/4608571/LHCSeminarArcangeletti\\_final.pdf](https://indico.cern.ch/event/1281604/attachments/2660420/4608571/LHCSeminarArcangeletti_final.pdf), 7<sup>th</sup> of June, 2023.
- [7] T. Biekötter, S. Heinemeyer and G. Weiglein, *95.4 GeV diphoton excess at ATLAS and CMS*, *Phys. Rev. D* **109** (2024) 035005 [[2306.03889](#)].
- [8] CMS collaboration, A. Tumasyan et al., *Searches for additional Higgs bosons and for vector leptoquarks in  $\tau\tau$  final states in proton-proton collisions at  $\sqrt{s} = 13$  TeV*, *JHEP* **07** (2023) 073 [[2208.02717](#)].
- [9] G. Coloretti, A. Crivellin, S. Bhattacharya and B. Mellado, *Searching for low-mass resonances decaying into W bosons*, *Phys. Rev. D* **108** (2023) 035026 [[2302.07276](#)].
- [10] CMS collaboration, A. Tumasyan et al., *Search for a new resonance decaying into two spin-0 bosons in a final state with two photons and two bottom quarks in proton-proton collisions at  $\sqrt{s} = 13$  TeV*, *JHEP* **05** (2024) 316 [[2310.01643](#)].
- [11] U. Ellwanger and C. Hugonie, *Additional Higgs Bosons near 95 and 650 GeV in the NMSSM*, *Eur. Phys. J. C* **83** (2023) 1138 [[2309.07838](#)].
- [12] CMS collaboration, A. Tumasyan et al., *Search for a heavy Higgs boson decaying into two lighter Higgs bosons in the  $\tau\tau bb$  final state at 13 TeV*, *JHEP* **11** (2021) 057 [[2106.10361](#)].
- [13] J.-W. Fan, J.-Q. Tao, Y.-Q. Shen, G.-M. Chen, H.-S. Chen, S. Gascon-Shotkin et al., *Study of diphoton decays of the lightest scalar Higgs boson in the Next-to-Minimal Supersymmetric Standard Model*, *Chin. Phys. C* **38** (2014) 073101 [[1309.6394](#)].
- [14] T. Biekötter, S. Heinemeyer and C. Muñoz, *Precise prediction for the Higgs-boson masses in the  $\mu\nu$  SSM*, *Eur. Phys. J. C* **78** (2018) 504 [[1712.07475](#)].
- [15] C. Beskidt, W. de Boer and D. I. Kazakov, *Can we discover a light singlet-like NMSSM Higgs boson at the LHC?*, *Phys. Lett. B* **782** (2018) 69 [[1712.02531](#)].
- [16] P. J. Fox and N. Weiner, *Light Signals from a Lighter Higgs*, *JHEP* **08** (2018) 025 [[1710.07649](#)].
- [17] U. Haisch and A. Malinauskas, *Let there be light from a second light Higgs doublet*, *JHEP* **03** (2018) 135 [[1712.06599](#)].
- [18] S. Heinemeyer and T. Stefaniak, *A Higgs Boson at 96 GeV?!*, *PoS CHARGED2018* (2019) 016 [[1812.05864](#)].
- [19] S. Heinemeyer, *A Higgs boson below 125 GeV?!*, *Int. J. Mod. Phys. A* **33** (2018) 1844006.

- [20] K. Wang, F. Wang, J. Zhu and Q. Jie, *The semi-constrained NMSSM in light of muon  $g-2$ , LHC, and dark matter constraints*, *Chin. Phys. C* **42** (2018) 103109 [1811.04435].
- [21] F. Domingo, S. Heinemeyer, S. Paßehr and G. Weiglein, *Decays of the neutral Higgs bosons into SM fermions and gauge bosons in the CP-violating NMSSM*, *Eur. Phys. J. C* **78** (2018) 942 [1807.06322].
- [22] R. Vega, R. Vega-Morales and K. Xie, *Light (and darkness) from a light hidden Higgs*, *JHEP* **06** (2018) 137 [1805.01970].
- [23] J. Cao, X. Jia, Y. Yue, H. Zhou and P. Zhu, *96 GeV diphoton excess in seesaw extensions of the natural NMSSM*, *Phys. Rev. D* **101** (2020) 055008 [1908.07206].
- [24] T. Biekötter, S. Heinemeyer and C. Muñoz, *Precise prediction for the Higgs-Boson masses in the  $\mu\nu$ SSM with three right-handed neutrino superfields*, *Eur. Phys. J. C* **79** (2019) 667 [1906.06173].
- [25] K. Choi, S. H. Im, K. S. Jeong and C. B. Park, *Light Higgs bosons in the general NMSSM*, *Eur. Phys. J. C* **79** (2019) 956 [1906.03389].
- [26] A. Kundu, S. Maharana and P. Mondal, *A 96 GeV scalar tagged to dark matter models*, *Nucl. Phys. B* **955** (2020) 115057 [1907.12808].
- [27] T. Biekötter, M. Chakraborti and S. Heinemeyer, *An N2HDM Solution for the possible 96 GeV Excess*, *PoS CORFU2018* (2019) 015 [1905.03280].
- [28] T. Biekötter, M. Chakraborti and S. Heinemeyer, *A 96 GeV Higgs boson in the N2HDM*, *Eur. Phys. J. C* **80** (2020) 2 [1903.11661].
- [29] D. Sachdeva and S. Sadhukhan, *Discussing 125 GeV and 95 GeV excess in light radion model*, *Phys. Rev. D* **101** (2020) 055045 [1908.01668].
- [30] T. Biekötter, M. Chakraborti and S. Heinemeyer, *The “96 GeV excess” at the LHC*, *Int. J. Mod. Phys. A* **36** (2021) 2142018 [2003.05422].
- [31] A. A. Abdelalim, B. Das, S. Khalil and S. Moretti, *Di-photon decay of a light Higgs state in the BLSSM*, *Nucl. Phys. B* **985** (2022) 116013 [2012.04952].
- [32] W. G. Hollik, C. Li, G. Moortgat-Pick and S. Paasch, *Phenomenology of a Supersymmetric Model Inspired by Inflation*, *Eur. Phys. J. C* **81** (2021) 141 [2004.14852].
- [33] J. A. Aguilar-Saavedra and F. R. Joaquim, *Multiphoton signals of a (96 GeV?) stealth boson*, *Eur. Phys. J. C* **80** (2020) 403 [2002.07697].
- [34] T. Biekötter, A. Grohsjean, S. Heinemeyer, C. Schwanenberger and G. Weiglein, *Possible indications for new Higgs bosons in the reach of the LHC: N2HDM and NMSSM interpretations*, *Eur. Phys. J. C* **82** (2022) 178 [2109.01128].
- [35] T. Biekötter and M. O. Olea-Romacho, *Reconciling Higgs physics and pseudo-Nambu-Goldstone dark matter in the S2HDM using a genetic algorithm*, *JHEP* **10** (2021) 215 [2108.10864].
- [36] S. Heinemeyer, C. Li, F. Lika, G. Moortgat-Pick and S. Paasch, *Phenomenology of a 96 GeV Higgs boson in the 2HDM with an additional singlet*, *Phys. Rev. D* **106** (2022) 075003 [2112.11958].
- [37] T. Biekötter, S. Heinemeyer and G. Weiglein, *Mounting evidence for a 95 GeV Higgs boson*, *JHEP* **08** (2022) 201 [2203.13180].

- [38] W. Li, H. Qiao and J. Zhu, *Light Higgs boson in the NMSSM confronted with the CMS di-photon and di-tau excesses\**, *Chin. Phys. C* **47** (2023) 123102 [2212.11739].
- [39] R. Benbrik, M. Boukidi and B. Manaut, *Interpreting the  $W$ -mass and muon  $(g_\mu - 2)$  anomalies within a 2-Higgs doublet model*, *Nucl. Phys. B* **1005** (2024) 116593 [2204.11755].
- [40] R. Benbrik, M. Boukidi, S. Moretti and S. Semmlali, *Explaining the 96 GeV Di-photon anomaly in a generic 2HDM Type-III*, *Phys. Lett. B* **832** (2022) 137245 [2204.07470].
- [41] C. Li, *Phenomenology of extended Two-Higgs-Doublets models*, Ph.D. thesis, Hamburg U., 2023. 10.3204/PUBDB-2023-03151.
- [42] T. Biekötter, S. Heinemeyer and G. Weiglein, *The CMS di-photon excess at 95 GeV in view of the LHC Run 2 results*, *Phys. Lett. B* **846** (2023) 138217 [2303.12018].
- [43] J. A. Aguilar-Saavedra, H. B. Câmara, F. R. Joaquim and J. F. Seabra, *Confronting the 95 GeV excesses within the UN2HDM*, **2307.03768**.
- [44] S. Banik, A. Crivellin, S. Iguro and T. Kitahara, *Asymmetric di-Higgs signals of the next-to-minimal 2HDM with a  $U(1)$  symmetry*, *Phys. Rev. D* **108** (2023) 075011 [2303.11351].
- [45] J. Dutta, J. Lahiri, C. Li, G. Moortgat-Pick, S. F. Tabira and J. A. Ziegler, *Dark matter phenomenology in 2HDMS in light of the 95 GeV excess*, *Eur. Phys. J. C* **84** (2024) 926 [2308.05653].
- [46] D. Borah, S. Mahapatra, P. K. Paul and N. Sahu, *Scotogenic  $U(1)_{L\mu-L\tau}$  origin of  $(g-2)_\mu$ ,  $W$ -mass anomaly and 95 GeV excess*, *Phys. Rev. D* **109** (2024) 055021 [2310.11953].
- [47] G. Arcadi, G. Busoni, D. Cabo-Almeida and N. Krishnan, *Is there a scalar or pseudoscalar at 95 GeV?*, *Phys. Rev. D* **110** (2024) 115028 [2311.14486].
- [48] A. Ahriche, *95 GeV excess in the Georgi-Machacek model: Single or twin peak resonance*, *Phys. Rev. D* **110** (2024) 035010 [2312.10484].
- [49] T.-K. Chen, C.-W. Chiang, S. Heinemeyer and G. Weiglein, *95 GeV Higgs boson in the Georgi-Machacek model*, *Phys. Rev. D* **109** (2024) 075043 [2312.13239].
- [50] P. S. B. Dev, R. N. Mohapatra and Y. Zhang, *Explanation of the 95 GeV  $\gamma\gamma$  and  $bb^-$  excesses in the minimal left-right symmetric model*, *Phys. Lett. B* **849** (2024) 138481 [2312.17733].
- [51] J. Cao, X. Jia, J. Lian and L. Meng, *95 GeV diphoton and  $bb^-$  excesses in the general next-to-minimal supersymmetric standard model*, *Phys. Rev. D* **109** (2024) 075001 [2310.08436].
- [52] A. Ahriche, M. L. Bellilet, M. O. Khojali, M. Kumar and A.-T. Mulaudzi, *Scale invariant scotogenic model: CDF-II  $W$ -boson mass and the 95 GeV excesses*, *Phys. Rev. D* **110** (2024) 015025 [2311.08297].
- [53] A. Belyaev, R. Benbrik, M. Boukidi, M. Chakraborti, S. Moretti and S. Semmlali, *Explanation of the hints for a 95 GeV Higgs boson within a 2-Higgs Doublet Model*, *JHEP* **05** (2024) 209 [2306.09029].
- [54] D. Azevedo, T. Biekötter and P. M. Ferreira, *2HDM interpretations of the CMS diphoton excess at 95 GeV*, *JHEP* **11** (2023) 017 [2305.19716].
- [55] S. Ashanujjaman, S. Banik, G. Coloretti, A. Crivellin, B. Mellado and A.-T. Mulaudzi,

- SU(2)<sub>L</sub> triplet scalar as the origin of the 95 GeV excess?*, *Phys. Rev. D* **108** (2023) L091704 [2306.15722].
- [56] A. Karan, V. Miralles and A. Pich, *Updated global fit of the aligned two-Higgs-doublet model with heavy scalars*, *Phys. Rev. D* **109** (2024) 035012 [2307.15419].
- [57] K. Wang and J. Zhu, *95 GeV light Higgs in the top-pair-associated diphoton channel at the LHC in the minimal dilaton model\**, *Chin. Phys. C* **48** (2024) 073105 [2402.11232].
- [58] U. Ellwanger and C. Hugonie, *Nmssm with correct relic density and an additional 95 GeV Higgs boson*, *Eur. Phys. J. C* **84** (2024) 526 [2403.16884].
- [59] J. Lian, *95 GeV excesses in the Z3-symmetric next-to-minimal supersymmetric standard model*, *Phys. Rev. D* **110** (2024) 115018 [2406.10969].
- [60] J. Cao, X. Jia and J. Lian, *Unified interpretation of the muon  $g-2$  anomaly, the 95 GeV diphoton, and  $bb^-$  excesses in the general next-to-minimal supersymmetric standard model*, *Phys. Rev. D* **110** (2024) 115039 [2402.15847].
- [61] C.-X. Liu, Y. Zhou, X.-Y. Zheng, J. Ma, T.-F. Feng and H.-B. Zhang, *95 GeV excess in a CP-violating  $\mu$ -from- $\nu$  SSM*, *Phys. Rev. D* **109** (2024) 056001 [2402.00727].
- [62] U. Ellwanger, C. Hugonie, S. F. King and S. Moretti, *NMSSM explanation for excesses in the search for neutralinos and charginos and a 95 GeV Higgs boson*, *Eur. Phys. J. C* **84** (2024) 788 [2404.19338].
- [63] S. Yaser Ayazi, M. Hosseini, S. Paktinat Mehdiabadi and R. Rouzbehi, *Vector dark matter and LHC constraints, including a 95 GeV light Higgs boson*, *Phys. Rev. D* **110** (2024) 055004 [2405.01132].
- [64] S. Gao, S.-M. Zhao, S. Di, X.-X. Dong and T.-F. Feng, *A 95 GeV Higgs boson in the U(1)<sub>X</sub>SSM*, *Nucl. Phys. B* **1018** (2025) 117026 [2411.13261].
- [65] J. Gao, X.-F. Han, J. Ma, L. Wang and H. Xu, *95 GeV Higgs boson and spontaneous CP-violation at the finite temperature*, *Phys. Rev. D* **110** (2024) 115045 [2408.03705].
- [66] T. Mondal, S. Moretti and P. Sanyal, *On the CP Nature of the ‘95 GeV’ Anomalies*, 2412.00474.
- [67] A. Khanna, S. Moretti and A. Sarkar, *Explaining 95 (or so) GeV Anomalies in the 2-Higgs Doublet Model Type-I*, 2409.02587.
- [68] S. Baek, P. Ko, Y. Omura and C. Yu, *96 GeV scalar boson in the 2HDM with U(1)<sub>H</sub> gauge symmetry*, *Eur. Phys. J. C* **85** (2025) 908 [2412.02178].
- [69] Y. Dong, K. Wang and J. Zhu, *Probing a type I 2HDM light Higgs boson in the top-pair-associated diphoton channel*, *Phys. Rev. D* **112** (2025) 055013 [2410.13636].
- [70] J. Kalinowski and W. Kotlarski, *Interpreting 95 GeV di-photon/ $b\bar{b}$  excesses as a lightest Higgs boson of the MRSSM*, *JHEP* **07** (2024) 037 [2403.08720].
- [71] H. Xu, Y. Wang, X.-F. Han and L. Wang, *95 GeV Higgs boson and nano-Hertz gravitational waves from domain walls in the N2HDM*, 2505.03592.
- [72] G. Abbas, V. Singh and N. Singh, *Dark-technicolour at colliders*, 2504.21593.
- [73] Z. Li, N. Liu and B. Zhu, *Interplay of 95 GeV Diphoton Excess and Dark Matter in Supersymmetric Triplet Model*, 2504.21273.

- [74] X. Du, H. Liu and Q. Chang, *Interpretation of 95 GeV excess within the Georgi-Machacek model in light of positive definiteness constraints*, *Phys. Rev. D* **112** (2025) 015019 [[2502.06444](#)].
- [75] R. Benbrik, M. Boukidi, K. Kahime, S. Moretti, L. Rahili and B. Taki, *Exploring potential Higgs resonances at 650 GeV and 95 GeV in the 2HDM Type III*, *Phys. Lett. B* **868** (2025) 139688 [[2505.07811](#)].
- [76] R. Benbrik, M. Boukidi, K. Kahime, S. Moretti, L. Rahili and B. Taki, *Interpreting the 650 GeV and 95 GeV Higgs Anomalies in the N2HDM*, [2510.19605](#).
- [77] A. Khanna, S. Moretti and A. Sarkar, *Explaining 650 GeV and 95 GeV Anomalies in the 2-Higgs Doublet Model Type-I*, [2509.06017](#).
- [78] Q. Chang, X. Du and P. Zhu, *Unified interpretation of 95 GeV di-photon and di-tau Excesses in the Georgi-Machacek Model*, [2509.26155](#).
- [79] A. Hmissou, S. Moretti and L. Rahili, *Could the 650 GeV excess be a pseudoscalar of a three-Higgs-doublet model?*, *Phys. Rev. D* **112** (2025) 075049 [[2509.06232](#)].
- [80] Y. Dong, M. Ruan, K. Wang, H. Yang and J. Zhu, *Prospects for a 95 GeV Higgs Boson at Future Higgs Factories with Transformer Networks*, [2510.24662](#).
- [81] T.-K. Chen, C.-W. Chiang, S. Heinemeyer and G. Weiglein, *Interpretation of LHC excesses at 95 GeV and 152 GeV in an extended Georgi-Machacek model*, [2511.04796](#).
- [82] A. M. Coutinho, A. Karan, V. Miralles and A. Pich, *Light scalars within the CP-conserving Aligned-two-Higgs-doublet model*, *JHEP* **02** (2025) 057 [[2412.14906](#)].
- [83] P. Fayet, *Supergauge Invariant Extension of the Higgs Mechanism and a Model for the electron and Its Neutrino*, *Nucl. Phys. B* **90** (1975) 104.
- [84] P. Fayet, *Supersymmetry and Weak, Electromagnetic and Strong Interactions*, *Phys. Lett. B* **64** (1976) 159.
- [85] P. Fayet and S. Ferrara, *Supersymmetry*, *Phys. Rept.* **32** (1977) 249.
- [86] P. Fayet, *Spontaneously Broken Supersymmetric Theories of Weak, Electromagnetic and Strong Interactions*, *Phys. Lett. B* **69** (1977) 489.
- [87] G. R. Farrar and P. Fayet, *Phenomenology of the Production, Decay, and Detection of New Hadronic States Associated with Supersymmetry*, *Phys. Lett. B* **76** (1978) 575.
- [88] U. Ellwanger, C. Hugonie and A. M. Teixeira, *The Next-to-Minimal Supersymmetric Standard Model*, *Phys. Rept.* **496** (2010) 1 [[0910.1785](#)].
- [89] M. Maniatis, *The Next-to-Minimal Supersymmetric extension of the Standard Model reviewed*, *Int. J. Mod. Phys. A* **25** (2010) 3505 [[0906.0777](#)].
- [90] A. Hammad, R. Ramos, A. Chakraborty, P. Ko and S. Moretti, *Explaining Data Anomalies over the NMSSM Parameter Space with Deep Learning Techniques*, [2508.13912](#).
- [91] U. Ellwanger and A. M. Teixeira, *NMSSM with a singlino LSP: possible challenges for searches for supersymmetry at the LHC*, *JHEP* **10** (2014) 113 [[1406.7221](#)].
- [92] J. Cao, D. Li, J. Lian, Y. Yue and H. Zhou, *Singlino-dominated dark matter in general NMSSM*, *JHEP* **06** (2021) 176 [[2102.05317](#)].
- [93] J. Cao, L. Meng, Y. Yue, H. Zhou and P. Zhu, *Suppressing the scattering of WIMP dark*

- matter and nucleons in supersymmetric theories, *Phys. Rev. D* **101** (2020) 075003 [[1910.14317](#)].
- [94] U. Ellwanger, *A Higgs boson near 125 GeV with enhanced di-photon signal in the NMSSM*, *JHEP* **03** (2012) 044 [[1112.3548](#)].
- [95] M. Badziak, M. Olechowski and S. Pokorski, *New Regions in the NMSSM with a 125 GeV Higgs*, *JHEP* **06** (2013) 043 [[1304.5437](#)].
- [96] J.-J. Cao, Z.-X. Heng, J. M. Yang, Y.-M. Zhang and J.-Y. Zhu, *A SM-like Higgs near 125 GeV in low energy SUSY: a comparative study for MSSM and NMSSM*, *JHEP* **03** (2012) 086 [[1202.5821](#)].
- [97] U. Ellwanger, *Nonrenormalizable interactions from supergravity, quantum corrections and effective low-energy theories*, *Phys. Lett. B* **133** (1983) 187.
- [98] S. A. Abel, *Destabilizing divergences in the NMSSM*, *Nucl. Phys. B* **480** (1996) 55 [[hep-ph/9609323](#)].
- [99] C. F. Kolda, S. Pokorski and N. Polonsky, *Stabilized singlets in supergravity as a source of the  $\mu$  - parameter*, *Phys. Rev. Lett.* **80** (1998) 5263 [[hep-ph/9803310](#)].
- [100] C. Panagiotakopoulos and K. Tamvakis, *Stabilized NMSSM without domain walls*, *Phys. Lett. B* **446** (1999) 224 [[hep-ph/9809475](#)].
- [101] G. G. Ross and K. Schmidt-Hoberg, *The Fine-Tuning of the Generalised NMSSM*, *Nucl. Phys. B* **862** (2012) 710 [[1108.1284](#)].
- [102] H. M. Lee, S. Raby, M. Ratz, G. G. Ross, R. Schieren, K. Schmidt-Hoberg et al., *A unique  $Z_4^R$  symmetry for the MSSM*, *Phys. Lett. B* **694** (2011) 491 [[1009.0905](#)].
- [103] H. M. Lee, S. Raby, M. Ratz, G. G. Ross, R. Schieren, K. Schmidt-Hoberg et al., *Discrete R symmetries for the MSSM and its singlet extensions*, *Nucl. Phys. B* **850** (2011) 1 [[1102.3595](#)].
- [104] G. G. Ross, K. Schmidt-Hoberg and F. Staub, *The Generalised NMSSM at One Loop: Fine Tuning and Phenomenology*, *JHEP* **08** (2012) 074 [[1205.1509](#)].
- [105] D. J. Miller, R. Nevzorov and P. M. Zerwas, *The Higgs sector of the next-to-minimal supersymmetric standard model*, *Nucl. Phys. B* **681** (2004) 3 [[hep-ph/0304049](#)].
- [106] M. Carena, H. E. Haber, I. Low, N. R. Shah and C. E. M. Wagner, *Alignment limit of the NMSSM Higgs sector*, *Phys. Rev. D* **93** (2016) 035013 [[1510.09137](#)].
- [107] ATLAS collaboration, G. Aad et al., *Search for heavy Higgs bosons decaying into two tau leptons with the ATLAS detector using pp collisions at  $\sqrt{s} = 13$  TeV*, *Phys. Rev. Lett.* **125** (2020) 051801 [[2002.12223](#)].
- [108] ATLAS collaboration, *A detailed map of Higgs boson interactions by the ATLAS experiment ten years after the discovery*, *Nature* **607** (2022) 52 [[2207.00092](#)].
- [109] CMS collaboration, A. Tumasyan et al., *A portrait of the Higgs boson by the CMS experiment ten years after the discovery*, *Nature* **607** (2022) 60 [[2207.00043](#)].
- [110] S. Baum, M. Carena, N. R. Shah and C. E. M. Wagner, *Higgs portals for thermal Dark Matter. EFT perspectives and the NMSSM*, *JHEP* **04** (2018) 069 [[1712.09873](#)].
- [111] L. Meng, J. Cao, F. Li and S. Yang, *Dark Matter physics in general NMSSM*, *JHEP* **08** (2024) 212 [[2405.07036](#)].

- [112] P. Huang and C. E. M. Wagner, *Blind Spots for neutralino Dark Matter in the MSSM with an intermediate  $m_A$* , *Phys. Rev. D* **90** (2014) 015018 [[1404.0392](#)].
- [113] A. Crivellin, M. Hoferichter, M. Procura and L. C. Tunstall, *Light stops, blind spots, and isospin violation in the MSSM*, *JHEP* **07** (2015) 129 [[1503.03478](#)].
- [114] T. Han, F. Kling, S. Su and Y. Wu, *Unblinding the dark matter blind spots*, *JHEP* **02** (2017) 057 [[1612.02387](#)].
- [115] M. Carena, J. Osborne, N. R. Shah and C. E. M. Wagner, *Supersymmetry and LHC Missing Energy Signals*, *Phys. Rev. D* **98** (2018) 115010 [[1809.11082](#)].
- [116] W. Abdallah, A. Datta and S. Roy, *A relatively light, highly bino-like dark matter in the  $Z_3$ -symmetric NMSSM and recent LHC searches*, *JHEP* **04** (2021) 122 [[2012.04026](#)].
- [117] A. Chatterjee, A. Datta and S. Roy, *Electroweak phase transition in the  $Z_3$ -invariant NMSSM: Implications of LHC and Dark matter searches and prospects of detecting the gravitational waves*, *JHEP* **06** (2022) 108 [[2202.12476](#)].
- [118] A. Datta, M. Guchait, A. Roy and S. Roy, *Hunting ewinos and a light scalar of  $Z_3$ -NMSSM with a bino-like dark matter in top squark decays at the LHC*, *JHEP* **11** (2023) 081 [[2211.05905](#)].
- [119] S. Roy and C. E. M. Wagner, *Dark Matter searches with photons at the LHC*, *JHEP* **04** (2024) 106 [[2401.08917](#)].
- [120] E. Arganda, M. de los Rios, A. D. Perez, S. Roy, R. M. Sandá Seoane and C. E. M. Wagner, *Shedding Light on Dark Matter at the LHC with Machine Learning*, [2509.15121](#).
- [121] H. Zhou and G. Ban, *Status of the  $Z_3$ -NMSSM featuring a light bino-dominated LSP and a light singletlike scalar under the LZ experiment*, *Phys. Rev. D* **112** (2025) 035001 [[2502.14664](#)].
- [122] F. Staub, *SARAH*, [0806.0538](#).
- [123] F. Staub, *SARAH 3.2: Dirac Gauginos, UFO output, and more*, *Comput. Phys. Commun.* **184** (2013) 1792 [[1207.0906](#)].
- [124] F. Staub, *SARAH 4 : A tool for (not only SUSY) model builders*, *Comput. Phys. Commun.* **185** (2014) 1773 [[1309.7223](#)].
- [125] F. Staub, *Exploring new models in all detail with SARAH*, *Adv. High Energy Phys.* **2015** (2015) 840780 [[1503.04200](#)].
- [126] W. Porod, *SPheno, a program for calculating supersymmetric spectra, SUSY particle decays and SUSY particle production at  $e^+ e^-$  colliders*, *Comput. Phys. Commun.* **153** (2003) 275 [[hep-ph/0301101](#)].
- [127] W. Porod and F. Staub, *SPheno 3.1: Extensions including flavour, CP-phases and models beyond the MSSM*, *Comput. Phys. Commun.* **183** (2012) 2458 [[1104.1573](#)].
- [128] W. Porod, F. Staub and A. Vicente, *A Flavor Kit for BSM models*, *Eur. Phys. J. C* **74** (2014) 2992 [[1405.1434](#)].
- [129] G. Belanger, F. Boudjema, A. Pukhov and A. Semenov, *MicrOMEGAs: A Program for calculating the relic density in the MSSM*, *Comput. Phys. Commun.* **149** (2002) 103 [[hep-ph/0112278](#)].
- [130] G. Bélanger, F. Boudjema, A. Pukhov and A. Semenov, *micrOMEGAs: Version 1.3*, *Comput. Phys. Commun.* **174** (2006) 577 [[hep-ph/0405253](#)].

- [131] G. Bélanger, F. Boudjema, C. Hugonie, A. Pukhov and A. Semenov, *Relic density of dark matter in the NMSSM*, *JCAP* **09** (2005) 001 [[hep-ph/0505142](#)].
- [132] G. Bélanger, F. Boudjema, A. Pukhov and A. Semenov, *MicrOMEGAs 2.0: A Program to calculate the relic density of dark matter in a generic model*, *Comput. Phys. Commun.* **176** (2007) 367 [[hep-ph/0607059](#)].
- [133] G. Bélanger, F. Boudjema, S. Kraml, A. Pukhov and A. Semenov, *Relic density of neutralino dark matter in the MSSM with CP violation*, *Phys. Rev. D* **73** (2006) 115007 [[hep-ph/0604150](#)].
- [134] G. Bélanger, F. Boudjema, A. Pukhov and A. Semenov, *Dark matter direct detection rate in a generic model with micrOMEGAs 2.2*, *Comput. Phys. Commun.* **180** (2009) 747 [[0803.2360](#)].
- [135] G. Belanger, F. Boudjema, A. Pukhov and A. Semenov, *micrOMEGAs: A Tool for dark matter studies*, *Nuovo Cim. C* **033N2** (2010) 111 [[1005.4133](#)].
- [136] Bélanger, G. and Boudjema, F. and Pukhov, A. and Semenov, A., *micrOMEGAs\_3: A program for calculating dark matter observables*, *Comput. Phys. Commun.* **185** (2014) 960 [[1305.0237](#)].
- [137] D. Barducci, G. Belanger, J. Bernon, F. Boudjema, J. Da Silva, S. Kraml et al., *Collider limits on new physics within micrOMEGAs\_4.3*, *Comput. Phys. Commun.* **222** (2018) 327 [[1606.03834](#)].
- [138] G. Bélanger, F. Boudjema, A. Goudelis, A. Pukhov and B. Zaldivar, *micrOMEGAs5.0 : Freeze-in*, *Comput. Phys. Commun.* **231** (2018) 173 [[1801.03509](#)].
- [139] A. Fowlie and M. H. Bardsley, *Superplot: a graphical interface for plotting and analysing MultiNest output*, *Eur. Phys. J. Plus* **131** (2016) 391 [[1603.00555](#)].
- [140] S. F. King and P. L. White, *Resolving the constrained minimal and next-to-minimal supersymmetric standard models*, *Phys. Rev. D* **52** (1995) 4183 [[hep-ph/9505326](#)].
- [141] M. Masip, R. Muñoz-Tapia and A. Pomarol, *Limits on the mass of the lightest Higgs in supersymmetric models*, *Phys. Rev. D* **57** (1998) R5340 [[hep-ph/9801437](#)].
- [142] F. Feroz, M. P. Hobson and M. Bridges, *MultiNest: an efficient and robust Bayesian inference tool for cosmology and particle physics*, *Mon. Not. Roy. Astron. Soc.* **398** (2009) 1601 [[0809.3437](#)].
- [143] F. Feroz, M. P. Hobson, E. Cameron and A. N. Pettitt, *Importance Nested Sampling and the MultiNest Algorithm*, *Open J. Astrophys.* **2** (2019) 10 [[1306.2144](#)].
- [144] P. Bechtle, S. Heinemeyer, O. Stål, T. Stefaniak and G. Weiglein, *HiggsSignals: Confronting arbitrary Higgs sectors with measurements at the Tevatron and the LHC*, *Eur. Phys. J. C* **74** (2014) 2711 [[1305.1933](#)].
- [145] O. Stål and T. Stefaniak, *Constraining extended Higgs sectors with HiggsSignals*, *PoS EPS-HEP2013* (2013) 314 [[1310.4039](#)].
- [146] P. Bechtle, S. Heinemeyer, O. Stål, T. Stefaniak and G. Weiglein, *Probing the Standard Model with Higgs signal rates from the Tevatron, the LHC and a future ILC*, *JHEP* **11** (2014) 039 [[1403.1582](#)].
- [147] P. Bechtle, S. Heinemeyer, T. Klingl, T. Stefaniak, G. Weiglein and J. Wittbrodt,

- HiggsSignals-2: Probing new physics with precision Higgs measurements in the LHC 13 TeV era*, *Eur. Phys. J. C* **81** (2021) 145 [2012.09197].
- [148] M. Mühlleitner, M. O. P. Sampaio, R. Santos and J. Wittbrodt, *ScannerS: parameter scans in extended scalar sectors*, *Eur. Phys. J. C* **82** (2022) 198 [2007.02985].
- [149] H. Bahl, T. Biekötter, S. Heinemeyer, C. Li, S. Paasch, G. Weiglein et al., *HiggsTools: BSM scalar phenomenology with new versions of HiggsBounds and HiggsSignals*, *Comput. Phys. Commun.* **291** (2023) 108803 [2210.09332].
- [150] P. Bechtle, O. Brein, S. Heinemeyer, G. Weiglein and K. E. Williams, *HiggsBounds: Confronting Arbitrary Higgs Sectors with Exclusion Bounds from LEP and the Tevatron*, *Comput. Phys. Commun.* **181** (2010) 138 [0811.4169].
- [151] P. Bechtle, O. Brein, S. Heinemeyer, G. Weiglein and K. E. Williams, *HiggsBounds 2.0.0: Confronting Neutral and Charged Higgs Sector Predictions with Exclusion Bounds from LEP and the Tevatron*, *Comput. Phys. Commun.* **182** (2011) 2605 [1102.1898].
- [152] P. Bechtle, O. Brein, S. Heinemeyer, O. Stal, T. Stefaniak, G. Weiglein et al., *Recent Developments in HiggsBounds and a Preview of HiggsSignals*, *PoS CHARGED2012* (2012) 024 [1301.2345].
- [153] P. Bechtle, O. Brein, S. Heinemeyer, O. Stål, T. Stefaniak, G. Weiglein et al., *HiggsBounds – 4: Improved Tests of Extended Higgs Sectors against Exclusion Bounds from LEP, the Tevatron and the LHC*, *Eur. Phys. J. C* **74** (2014) 2693 [1311.0055].
- [154] P. Bechtle, D. Dercks, S. Heinemeyer, T. Klingl, T. Stefaniak, G. Weiglein et al., *HiggsBounds-5: Testing Higgs Sectors in the LHC 13 TeV Era*, *Eur. Phys. J. C* **80** (2020) 1211 [2006.06007].
- [155] PLANCK collaboration, N. Aghanim et al., *Planck 2018 results. VI. Cosmological parameters*, *Astron. Astrophys.* **641** (2020) A6 [1807.06209].
- [156] LZ collaboration, J. Aalbers et al., *Dark Matter Search Results from 4.2 Tonne-Years of Exposure of the LUX-ZEPLIN (LZ) Experiment*, *Phys. Rev. Lett.* **135** (2025) 011802 [2410.17036].
- [157] S. Haselschwardt, “New dark matter search results from the lux-zeplin (lz) experiment.” [https://indico.uchicago.edu/event/427/contributions/1325/attachments/359/548/lz\\_results\\_tevpa.pdf](https://indico.uchicago.edu/event/427/contributions/1325/attachments/359/548/lz_results_tevpa.pdf), 2024.
- [158] FERMI-LAT collaboration, M. Ackermann et al., *Searching for Dark Matter Annihilation from Milky Way Dwarf Spheroidal Galaxies with Six Years of Fermi Large Area Telescope Data*, *Phys. Rev. Lett.* **115** (2015) 231301 [1503.02641].
- [159] PARTICLE DATA GROUP collaboration, S. Navas et al., *Review of particle physics*, *Phys. Rev. D* **110** (2024) 030001.
- [160] W. G. Hollik, G. Weiglein and J. Wittbrodt, *Impact of Vacuum Stability Constraints on the Phenomenology of Supersymmetric Models*, *JHEP* **03** (2019) 109 [1812.04644].
- [161] B. O’Leary and J. E. Camargo-Molina, “VevaciousPlusPlus.” <https://github.com/JoseElie1/VevaciousPlusPlus>, 2014.
- [162] J. E. Camargo-Molina, B. O’Leary, W. Porod and F. Staub, *Vevacious: A Tool For Finding The Global Minima Of One-Loop Effective Potentials With Many Scalars*, *Eur. Phys. J. C* **73** (2013) 2588 [1307.1477].

- [163] ATLAS collaboration, G. Aad et al., *A statistical combination of ATLAS Run 2 searches for charginos and neutralinos at the LHC*, [2402.08347](#).
- [164] C. K. Khosa, S. Kraml, A. Lessa, P. Neuhuber and W. Waltenberger, *SModelS database update v1.2.3*, [2005.00555](#).
- [165] J. Alwall, M. Herquet, F. Maltoni, O. Mattelaer and T. Stelzer, *MadGraph 5 : Going Beyond*, *JHEP* **06** (2011) 128 [[1106.0522](#)].
- [166] E. Conte, B. Fuks and G. Serret, *MadAnalysis 5, A User-Friendly Framework for Collider Phenomenology*, *Comput. Phys. Commun.* **184** (2013) 222 [[1206.1599](#)].
- [167] W. Beenakker, R. Hopker and M. Spira, *PROSPINO: A Program for the production of supersymmetric particles in next-to-leading order QCD*, [hep-ph/9611232](#).
- [168] T. Sjöstrand, S. Ask, J. R. Christiansen, R. Corke, N. Desai, P. Ilten et al., *An introduction to PYTHIA 8.2*, *Comput. Phys. Commun.* **191** (2015) 159 [[1410.3012](#)].
- [169] DELPHES 3 collaboration, J. de Favereau, C. Delaere, P. Demin, A. Giammanco, V. Lemaitre, A. Mertens et al., *DELPHES 3, A modular framework for fast simulation of a generic collider experiment*, *JHEP* **02** (2014) 057 [[1307.6346](#)].
- [170] M. Drees, H. Dreiner, D. Schmeier, J. Tattersall and J. S. Kim, *CheckMATE: Confronting your Favourite New Physics Model with LHC Data*, *Comput. Phys. Commun.* **187** (2015) 227 [[1312.2591](#)].
- [171] D. Dercks, N. Desai, J. S. Kim, K. Rolbiecki, J. Tattersall and T. Weber, *CheckMATE 2: From the model to the limit*, *Comput. Phys. Commun.* **221** (2017) 383 [[1611.09856](#)].
- [172] J. S. Kim, D. Schmeier, J. Tattersall and K. Rolbiecki, *A framework to create customised LHC analyses within CheckMATE*, *Comput. Phys. Commun.* **196** (2015) 535 [[1503.01123](#)].
- [173] J. Cao, J. Lian, Y. Pan, D. Zhang and P. Zhu, *Improved  $(g - 2)_\mu$  measurement and singlino dark matter in  $\mu$ -term extended  $Z_3$ -NMSSM*, *JHEP* **09** (2021) 175 [[2104.03284](#)].
- [174] F. Feroz and M. P. Hobson, *Multimodal nested sampling: an efficient and robust alternative to MCMC methods for astronomical data analysis*, *Mon. Not. Roy. Astron. Soc.* **384** (2008) 449 [[0704.3704](#)].
- [175] J. Skilling, *Nested sampling for general Bayesian computation*, *Bayesian Analysis* **1** (2006) 833.
- [176] CMS collaboration, A. M. Sirunyan et al., *Search for a heavy pseudoscalar boson decaying to a Z and a Higgs boson at  $\sqrt{s} = 13$  TeV*, *Eur. Phys. J. C* **79** (2019) 564 [[1903.00941](#)].
- [177] ATLAS collaboration, G. Aad et al., *Search for heavy resonances decaying into a Z or W boson and a Higgs boson in final states with leptons and b-jets in  $139 \text{ fb}^{-1}$  of pp collisions at  $\sqrt{s} = 13$  TeV with the ATLAS detector*, *JHEP* **06** (2023) 016 [[2207.00230](#)].
- [178] CMS collaboration, A. M. Sirunyan et al., *Search for new neutral Higgs bosons through the  $H \rightarrow ZA \rightarrow \ell^+ \ell^- b \bar{b}$  process in pp collisions at  $\sqrt{s} = 13$  TeV*, *JHEP* **03** (2020) 055 [[1911.03781](#)].
- [179] CMS collaboration, A. M. Sirunyan et al., *Search for heavy Higgs bosons decaying to a top quark pair in proton-proton collisions at  $\sqrt{s} = 13$  TeV*, *JHEP* **04** (2020) 171 [[1908.01115](#)].
- [180] LZ collaboration, D. S. Akerib et al., *Projected WIMP sensitivity of the LUX-ZEPLIN dark matter experiment*, *Phys. Rev. D* **101** (2020) 052002 [[1802.06039](#)].

- [181] J. Billard, L. Strigari and E. Figueroa-Feliciano, *Implication of neutrino backgrounds on the reach of next generation dark matter direct detection experiments*, *Phys. Rev. D* **89** (2014) 023524 [[1307.5458](#)].
- [182] CMS collaboration, A. M. Sirunyan et al., *Search for electroweak production of charginos and neutralinos in multilepton final states in proton-proton collisions at  $\sqrt{s} = 13$  TeV*, *JHEP* **03** (2018) 166 [[1709.05406](#)].
- [183] ATLAS collaboration, G. Aad et al., *Searches for electroweak production of supersymmetric particles with compressed mass spectra in  $\sqrt{s} = 13$  TeV pp collisions with the ATLAS detector*, *Phys. Rev. D* **101** (2020) 052005 [[1911.12606](#)].
- [184] CMS collaboration, A. M. Sirunyan et al., *Search for supersymmetry in final states with two oppositely charged same-flavor leptons and missing transverse momentum in proton-proton collisions at  $\sqrt{s} = 13$  TeV*, *JHEP* **04** (2021) 123 [[2012.08600](#)].
- [185] ATLAS collaboration, G. Aad et al., *Search for chargino-neutralino pair production in final states with three leptons and missing transverse momentum in  $\sqrt{s} = 13$  TeV pp collisions with the ATLAS detector*, *Eur. Phys. J. C* **81** (2021) 1118 [[2106.01676](#)].
- [186] CMS collaboration, A. M. Sirunyan et al., *Combined search for electroweak production of charginos and neutralinos in proton-proton collisions at  $\sqrt{s} = 13$  TeV*, *JHEP* **03** (2018) 160 [[1801.03957](#)].
- [187] ATLAS collaboration, M. Aaboud et al., *Search for electroweak production of supersymmetric particles in final states with two or three leptons at  $\sqrt{s} = 13$  TeV with the ATLAS detector*, *Eur. Phys. J. C* **78** (2018) 995 [[1803.02762](#)].
- [188] ATLAS collaboration, M. Aaboud et al., *Search for chargino-neutralino production using recursive jigsaw reconstruction in final states with two or three charged leptons in proton-proton collisions at  $\sqrt{s} = 13$  TeV with the ATLAS detector*, *Phys. Rev. D* **98** (2018) 092012 [[1806.02293](#)].
- [189] ATLAS collaboration, G. Aad et al., *Search for direct production of electroweakinos in final states with one lepton, missing transverse momentum and a Higgs boson decaying into two b-jets in pp collisions at  $\sqrt{s} = 13$  TeV with the ATLAS detector*, *Eur. Phys. J. C* **80** (2020) 691 [[1909.09226](#)].
- [190] ATLAS collaboration, M. Aaboud et al., *Search for chargino and neutralino production in final states with a Higgs boson and missing transverse momentum at  $\sqrt{s} = 13$  TeV with the ATLAS detector*, *Phys. Rev. D* **100** (2019) 012006 [[1812.09432](#)].
- [191] CMS collaboration, A. M. Sirunyan et al., *Search for new phenomena in final states with two opposite-charge, same-flavor leptons, jets, and missing transverse momentum in pp collisions at  $\sqrt{s} = 13$  TeV*, *JHEP* **03** (2018) 076 [[1709.08908](#)].
- [192] CMS collaboration, A. M. Sirunyan et al., *Search for supersymmetry with Higgs boson to diphoton decays using the razor variables at  $\sqrt{s} = 13$  TeV*, *Phys. Lett. B* **779** (2018) 166 [[1709.00384](#)].
- [193] ATLAS collaboration, G. Aad et al., *Search for electroweak production of charginos and sleptons decaying into final states with two leptons and missing transverse momentum in  $\sqrt{s} = 13$  TeV pp collisions using the ATLAS detector*, *Eur. Phys. J. C* **80** (2020) 123 [[1908.08215](#)].
- [194] CMS collaboration, A. M. Sirunyan et al., *Searches for pair production of charginos and*

*top squarks in final states with two oppositely charged leptons in proton-proton collisions at  $\sqrt{s} = 13$  TeV*, *JHEP* **11** (2018) 079 [[1807.07799](#)].

- [195] ATLAS collaboration, G. Aad et al., *Search for charginos and neutralinos in final states with two boosted hadronically decaying bosons and missing transverse momentum in pp collisions at  $\sqrt{s} = 13$  TeV with the ATLAS detector*, *Phys. Rev. D* **104** (2021) 112010 [[2108.07586](#)].
- [196] ATLAS collaboration, M. Aaboud et al., *Search for photonic signatures of gauge-mediated supersymmetry in 13 TeV pp collisions with the ATLAS detector*, *Phys. Rev. D* **97** (2018) 092006 [[1802.03158](#)].
- [197] ATLAS collaboration, G. Aad et al., *Search for supersymmetry in events with four or more charged leptons in  $139\text{fb}^{-1}$  of  $\sqrt{s} = 13$  TeV pp collisions with the ATLAS detector*, *JHEP* **07** (2021) 167 [[2103.11684](#)].
- [198] ATLAS collaboration, M. Aaboud et al., *Search for electroweak production of supersymmetric states in scenarios with compressed mass spectra at  $\sqrt{s} = 13$  TeV with the ATLAS detector*, *Phys. Rev. D* **97** (2018) 052010 [[1712.08119](#)].
- [199] CMS collaboration, A. M. Sirunyan et al., *Search for new physics in events with two soft oppositely charged leptons and missing transverse momentum in proton-proton collisions at  $\sqrt{s} = 13$  TeV*, *Phys. Lett. B* **782** (2018) 440 [[1801.01846](#)].